Supplementary Information to Tracer Trajectories and Displacement due to a Micro-Swimmer near a Surface

A.J.Th.M. Mathijssen[1]†, D.O. Pushkin[1] and J.M. Yeomans[1]

[1]Rudolf Peierls Centre for Theoretical Physics, University of Oxford, 1 Keble Road, Oxford, OX1 3NP, UK

(Received 4 May 2015)

CONTENTS

1. Mathematical model: flow field 2
- 1.1. The Stokeslet 2
- 1.2. The multipole expansion 2
- 1.3. Determining the flow field components 3

2. Mathematical model: flow field in a semi-infinite fluid 8
- 2.1. Image system for a free-slip boundary 8
- 2.2. Image system for a no-slip boundary 9
- 2.3. Multipole expansion in a semi-infinite fluid 9
- 2.4. Effective Stokeslets 10
- 2.5. Flow field for a free-slip boundary 10
- 2.6. Flow field for a no-slip boundary 11

3. Computing the separatrix 12
- 3.1. The flow field stream function 12
- 3.2. Definition of the separatrix 12
- 3.3. Solution for a quadrupolar swimmer 13
- 3.4. Solution for a swimmer with dipolar plus quadrupolar flow field. 13

4. Integrating the tracer equations of motion 14
- 4.1. Micro-swimmer in an unbounded fluid 14
- 4.2. Micro-swimmer near a no-slip boundary 16
- 4.3. Micro-swimmer near a free-slip boundary 19

5. Analytical results: swimmer moving parallel to a free-slip boundary 20
- 5.1. Longitudinal component of the tracer displacement 21
- 5.2. Transverse components of the tracer displacement 22

6. Analytical results: swimmer moving parallel to a no-slip boundary 24
- 6.1. Longitudinal component of the tracer displacement 25
- 6.2. Transverse components of the tracer displacement 26

† Email address for correspondence: mathijssen@physics.ox.ac.uk

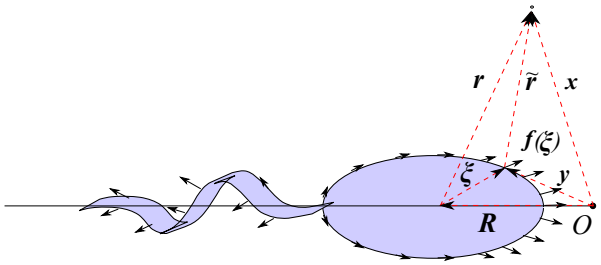

Figure 1: Geometry diagram for a swimmer in an infinite fluid. The swimmer generates a distribution of forces $\boldsymbol{f}(\boldsymbol{\xi})$ over its surface $S(\boldsymbol{\xi})$ acting on the fluid, and hence induces a fluid velocity field $u^{sw}(\boldsymbol{r})$.

1. Mathematical model: flow field

1.1. *The Stokeslet*

The hydrodynamics of an incompressible, zero Reynolds number fluid is described by the Stokes equations:

$$0 = -\boldsymbol{\nabla} p(\boldsymbol{x},t) + \mu \nabla^2 \boldsymbol{u}(\boldsymbol{x},t) + \boldsymbol{F}(\boldsymbol{x}), \tag{1.1}$$

$$0 = \boldsymbol{\nabla} \cdot \boldsymbol{u}(\boldsymbol{x},t), \tag{1.2}$$

where $\boldsymbol{u}(\boldsymbol{x},t)$ is the velocity field of the fluid at location $\boldsymbol{x}$ and time t, $p(\boldsymbol{x},t)$ is the pressure, μ is the dynamic viscosity and $\boldsymbol{F}(\boldsymbol{x}) = f_j \hat{\boldsymbol{e}}_j$ is any external force, where $\hat{\boldsymbol{e}}_j$ are unit vectors and j denotes the Cartesian directions $j \in \{x, y, z\}$.

Consider a point force $\boldsymbol{F}^S(\boldsymbol{x},\boldsymbol{y}) = \delta^3(\boldsymbol{x}-\boldsymbol{y})\boldsymbol{f}^S$ acting at the point $\boldsymbol{y}$, where $\delta^3(\boldsymbol{x})$ is the Dirac delta function and $\boldsymbol{f}^S$ is the force strength. This geometry is shown in figure 1. The fundamental singular solution in three dimensions of Stokes' equations for the fluid velocity field $\boldsymbol{u}^S$ at the point $\tilde{\boldsymbol{r}} = \boldsymbol{x} - \boldsymbol{y}$ due to the point force $\boldsymbol{F}^S$ is

$$u_i^S(\tilde{\boldsymbol{r}}, \boldsymbol{f}^S) = f_j^S \cdot \mathcal{G}_{ij}(\tilde{\boldsymbol{r}}), \tag{1.3}$$

$$\mathcal{G}_{ij}(\boldsymbol{r}) = \frac{1}{8\pi\mu}\left(\frac{\delta_{ij}}{r} + \frac{r_i r_j}{r^3}\right), \tag{1.4}$$

where $\mathcal{G}_{ij}(\boldsymbol{r})$ is the Green's function known as the Oseen tensor, δ_{ij} is the Kronecker delta and $r = |\boldsymbol{r}|$. The resulting velocity field, called the Stokeslet, is shown in figure 2a.

The corresponding pressure field due to the point force $\boldsymbol{F}^S$ has a similar singularity solution:

$$p(\tilde{\boldsymbol{r}}, \boldsymbol{f}^S) = \tilde{f}_j^S \cdot \mathcal{P}_j(\tilde{\boldsymbol{r}}), \qquad \mathcal{P}_j(\boldsymbol{r}) = \frac{r_j}{4\pi r^3} = -\frac{1}{4\pi}\partial_j\left(\frac{1}{r}\right). \tag{1.5}$$

A complete account of Green's functions of Stokes flow is given by Pozrikidis (1992).

1.2. *The multipole expansion*

Consider a micro-swimmer located at position $\boldsymbol{R}$ with a surface S located at position $\boldsymbol{y} = \boldsymbol{R} + \boldsymbol{\xi}$. We define the relative position variable $\boldsymbol{r} = \boldsymbol{x} - \boldsymbol{R}$, as shown in figure 1.

By changing their shape, swimmers exert forces and torques on the fluid. We model these forces as a distribution of Stokeslets, $\boldsymbol{f}(\boldsymbol{\xi})$, summed over the swimmer's surface $S(\boldsymbol{\xi})$. Using equation (1.3), the flow field is then given by

$$u_i^{sw}(\boldsymbol{r}) = \int_{S(\boldsymbol{\xi})} \mathcal{G}_{ij}(\boldsymbol{r}-\boldsymbol{\xi}) f_j(\boldsymbol{\xi}) dS. \tag{1.6}$$

Performing a multipole expansion for small $\boldsymbol{\xi}$ values around the relative position $\boldsymbol{r}$ gives

$$u_i^{sw}(\boldsymbol{r}) = \int_S \left(\mathcal{G}_{ij}(\boldsymbol{r}) - \frac{\partial \mathcal{G}_{ij}(\boldsymbol{r})}{\partial r_k}\xi_k + \frac{1}{2}\frac{\partial^2 \mathcal{G}_{ij}(\boldsymbol{r})}{\partial r_k \partial r_l}\xi_k\xi_l + \dots \right) f_j(\boldsymbol{\xi}) dS. \tag{1.7}$$

The Oseen tensor and its derivatives are independent of $\boldsymbol{\xi}$, thus

$$u_i^{sw}(\boldsymbol{r}) = \mathcal{G}_{ij}\left(\int_S f_j dS\right) - \frac{\partial \mathcal{G}_{ij}}{\partial r_k}\left(\int_S f_j \xi_k dS\right) + \frac{1}{2}\frac{\partial^2 \mathcal{G}_{ij}}{\partial r_k \partial r_l}\left(\int_S f_j \xi_k \xi_l dS\right) + \dots, \tag{1.8}$$

where the arguments have been omitted for transparency. We identify the successive integral expressions as the force strength tensor F_j, dipole moment tensor D_{jk}, and the quadrupole moment tensor Q_{jkl} etc. Hence we obtain

$$u_i^{sw}(\boldsymbol{r}) = \mathcal{G}_{ij}\mathsf{F}_j - \mathcal{G}_{ijk}\mathsf{D}_{jk} + \frac{1}{2}\mathcal{G}_{ijkl}\mathsf{Q}_{jkl} - \frac{1}{3!}\mathcal{G}_{ijklm}\mathsf{O}_{jklm} + \dots, \tag{1.9}$$

where the multipole moment tensors are

$$\mathsf{F}_j = \int_S f_j dS, \qquad \mathsf{D}_{jk} = \int_S f_j \xi_k dS, \qquad \mathsf{Q}_{jkl} = \int_S f_j \xi_k \xi_l dS, \ \dots, \tag{1.10}$$

and where the dipole singularity tensor $\mathcal{G}_{ijk}$, the quadrupole singularity tensor $\mathcal{G}_{ijkl}$, etc. are successive derivatives of the Oseen tenson $\mathcal{G}_{ij}(\boldsymbol{r})$ with respect to $\boldsymbol{r}$. Therefore, the successive terms in equation (1.9) scale as r^{-1}, r^{-2}, r^{-3}, etc. A more detailed explanation of the multipole expansion can be found in Kim & Karilla (1991, p.27) or more explicitly in this context in the work by Yeomans *et al.* (2014).

Before we continue, notice that the SI physical units of $\mathcal{G}_{ij}$ and F_j are s/kg and $kg\ m/s^2$ respectively, combining to velocity unit m/s. If we absorb the factor of $1/(8\pi\mu)$ from the Stokeslet (1.4) into the multipole moments, then $\mathsf{F}_j/8\pi\mu$, $\mathsf{D}_{jk}/8\pi\mu$, and $\mathsf{Q}_{jkl}/8\pi\mu$ carry units $\mu\mathrm{m}^2/s$, $\mu\mathrm{m}^3/s$, and $\mu\mathrm{m}^4/s$ respectively.

1.3. *Determining the flow field components*

Many micro-swimmers have, to a good approximation, a shape that is cylindrically symmetric about the swimming direction. Here we will use the cylindrical symmetry of the swimmer to restrict the number of non-zero components of the swimmer multipole moments (1.10), and hence we derive expressions for the flow field components

$$\boldsymbol{u}^{sw}(\boldsymbol{r}, \hat{\boldsymbol{e}}_k) = \boldsymbol{u}^D(\boldsymbol{r}, \hat{\boldsymbol{e}}_k; \kappa) + \boldsymbol{u}^Q(\boldsymbol{r}, \hat{\boldsymbol{e}}_k; Q_{\parallel,\perp,r}) + \dots \tag{1.11}$$

in terms of a limited set of parameters, κ, $Q_\parallel$, $Q_\perp$, Q_r etc. . Figure 2 gives a pictorial summary of the flow generated by each of these contributions to the multipole expansion (1.9).

1.3.1. *Cylindrical symmetry*

Consider a micro-swimmer with a cylindrically symmetric shape about the swimming direction, $\hat{\boldsymbol{e}}_z$, as shown in figure 1. The swimmer is subject to a force distribution $f_j(\boldsymbol{\xi}) = f_j(\rho, z)$, where we use cylindrical coordinates so that

$$(\xi_x, \xi_y, \xi_z) = (\rho\cos\phi, \rho\sin\phi, z), \tag{1.12}$$

$$(f_x, f_y, f_z) = (\cos\phi f_\rho - \sin\phi f_\phi, \sin\phi f_\rho + \cos\phi f_\phi, f_z), \tag{1.13}$$

and the surface $S(\boldsymbol{\xi})$ may be parameterised with $\rho = \rho(z)$ so that the surface position $\boldsymbol{\xi} = \boldsymbol{\xi}(\phi, z)$ does not depend explicitly on ρ. The surface integral of an arbitrary function

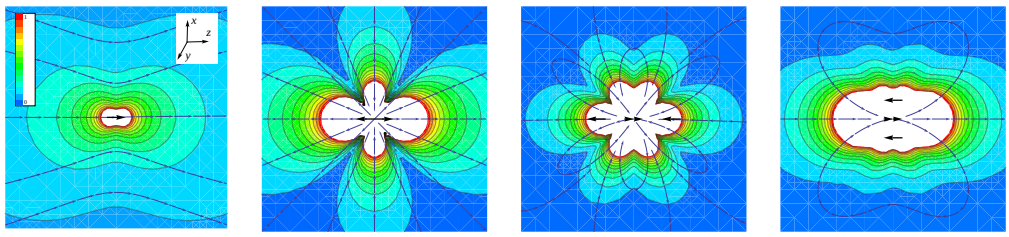

(a) Stokeslet $f_z = 1/5$ (b) Dipole $\kappa = 1$ (c) Quadrupole $Q_{\parallel} = 1$ (d) Quadrupole $Q_{\perp} = 1$

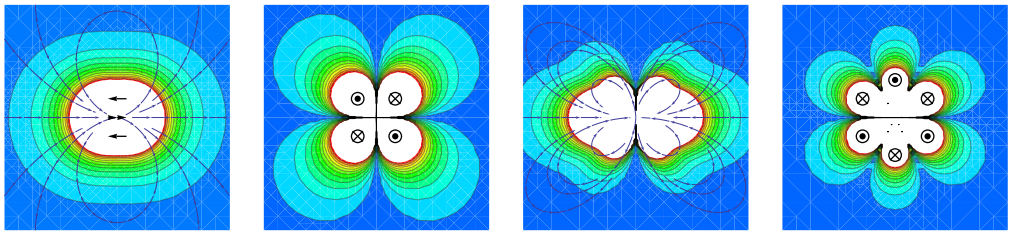

(e) Source doublet $Q_{\parallel} = 1, Q_{\perp} = 1$ (f) Rotlet doublet $Q_r = 1$ (g) Octupole $O_{\parallel} = 1, O_{\perp} = 1$ (h) Rotlet triplet $O_r = 1$

Figure 2: Flow fields produced by a micro-swimmer corresponding to different multipole expansion singularities, as seen in the (z, ρ) plane in the laboratory frame, where the swimmer is located at the origin and the swimming direction is from left to right. Colours portray the relative magnitude ranging from zero (blue) to unity (red) and white denotes the singularity center. Arrows indicate the velocity direction in the (z, ρ) plane, except in figures (*f, h*) where the direction is directly into and out of the plane indicated by the $\otimes$ and $\odot$ symbols respectively.

$g(\boldsymbol{\xi})$ can then be written as an integral over ϕ and z as

$$\int_S g(\boldsymbol{\xi}) dS = \int\int g(\boldsymbol{\xi}) J(z) d\phi dz, \qquad J(z) = \rho \sqrt{1 + \left(\frac{\partial \rho}{\partial z}\right)^2}, \tag{1.14}$$

where $J(z)$ is the Jacobian determinant for the surface S. For example, if the surface is a simple spherical shell of radius a_{sw} we have $J = a_{sw}$.

The integral over ϕ can now be performed for the multipole moments (1.10), noting that the force distribution $f_j(\rho, z)$ does not depend on ϕ, and hence the non-vanishing components of the flow field can determined. This is done for the dipolar, quadrupolar and octupolar moments in the following subsections.

1.3.2. *Force contribution*

Firstly, an autonomous swimmer cannot rely on external forces to move forwards. Therefore, assuming that the effects of gravity are negligible, the net force integrated over the swimmer surface must be zero so that the force strength tensor components all vanish, $F_j = 0$. This assumption is true for swimmers that are neutrally buoyant, or if their sedimentation velocity is negligible compared to their swimming speed (see Ishikawa *et al.* 2006).

1.3.3. *Dipolar contribution*

Since the net force on a naturally buoyant swimmer must vanish, the dipolar contribution to the velocity field, $u_i^D = D_{jk}\mathcal{G}_{ijk}$, is the leading order term in the multipole

expansion (1.9). The tensor D_{jk} contains 9 components, but in this section we show that the dipolar flow field $\boldsymbol{u}^D$ can be written in terms of only two independent parameters, corresponding to the stresslet and the rotlet term.

Because of the incompressibility of the flow field, $\boldsymbol{\nabla}\cdot\boldsymbol{u}^S = 0$, we obtain the identity

$$\delta_{jk}\mathcal{G}_{ijk} = 0 \tag{1.15}$$

$$\because\ \boldsymbol{\nabla}\cdot(f_j\mathcal{G}_{ij}) = f_j\mathcal{G}_{iji} = f_j\delta_{ik}\mathcal{G}_{ijk} = f_j\delta_{ik}\mathcal{G}_{jik} = f_i\delta_{jk}\mathcal{G}_{ijk} = 0\ \forall f_i. \tag{1.16}$$

Similarly, for higher orders we have

$$0 = \delta_{j\alpha}\mathcal{G}_{ij\ldots\alpha\ldots}. \tag{1.17}$$

The dipole moment tensor can therefore be made traceless by defining a new tensor $\tilde{\mathsf{D}}_{jk} = \mathsf{D}_{jk} - \frac{1}{3}\mathsf{D}_{ii}\delta_{jk}$ that gives the same flow field, i.e. $u_i^D = \tilde{\mathsf{D}}_{jk}\mathcal{G}_{ijk} = \mathsf{D}_{jk}\mathcal{G}_{ijk}$. We separate $\tilde{\mathsf{D}}$ into a symmeric part, called the stresslet tensor, and an antisymmetric part, $\tilde{\mathsf{D}}_{jk} = \mathsf{S}_{jk} + \mathsf{T}_{jk}$, where

$$\mathsf{S}_{jk} = \frac{1}{2}\int_S (f_j\xi_k + f_k\xi_j)dS - \frac{1}{3}\int_S f_i\xi_i dS\ \delta_{jk}, \tag{1.18}$$

$$\mathsf{T}_{jk} = \frac{1}{2}\int_S (f_j\xi_k - f_k\xi_j)dS. \tag{1.19}$$

We substitute equations (1.12) and (1.13) into these tensors (1.18) and (1.19). Using equation (1.14) we integrate over the ϕ co-ordinate and obtain

$$\mathsf{S}_{jk} = \begin{pmatrix} -a & 0 & 0 \\ 0 & -a & 0 \\ 0 & 0 & 2a \end{pmatrix}, \quad \mathsf{T}_{jk} = \begin{pmatrix} 0 & -b & 0 \\ b & 0 & 0 \\ 0 & 0 & 0 \end{pmatrix}, \tag{1.20}$$

$$a = 2\pi\int \frac{1}{6}(2zf_z - \rho f_\rho)Jdz, \tag{1.21}$$

$$b = 2\pi\int \frac{1}{2}\rho f_\phi Jdz. \tag{1.22}$$

The net torque exerted on the fluid is

$$T_i = -\int_S \varepsilon_{ijk}f_j\xi_k dS, \tag{1.23}$$

where ε_{jkl} is the Levi-Civita tensor. For a general T_{jk} tensor, given by equation (1.19), we can write the relations

$$\mathsf{T}_{jk} = -\frac{1}{2}T_\alpha\varepsilon_{\alpha jk}, \quad T_\alpha = -\varepsilon_{\alpha jk}\mathsf{T}_{jk}. \tag{1.24}$$

Therefore, the flow field due to a point torque, called the rotlet, is

$$u_i^T(\boldsymbol{r}) = -\mathsf{T}_{jk}\mathcal{G}_{ijk} = \frac{1}{2}T_\alpha\varepsilon_{\alpha jk}\mathcal{G}_{ijk}. \tag{1.25}$$

Since the Oseen tensor obeys the identity

$$\varepsilon_{\alpha jk}\mathcal{G}_{ijk} = -\varepsilon_{ijk}\mathcal{G}_{\alpha jk}, \tag{1.26}$$

the rotlet (1.25) can be rewritten in terms of the Stokeslets $\boldsymbol{u}_\alpha^S = \boldsymbol{u}^S(\boldsymbol{r}, \hat{\boldsymbol{e}}_\alpha)$ as

$$u_i^T(\boldsymbol{r}) = \frac{1}{2}T_\alpha\varepsilon_{ikj}\mathcal{G}_{j\alpha k} = \frac{1}{2}T_\alpha\left(\boldsymbol{\nabla}\times\boldsymbol{u}_\alpha^S\right)_i. \tag{1.27}$$

For a cylindrically symmetric force distribution, we substitute equation (1.22) into (1.24)

to obtain $T_z = 2b$. If we consider swimmers with zero net torque, however, we require that $b = 0$.

The stresslet tensor may be rewritten as $\tilde{\mathsf{S}}_{jk} = \mathsf{S}_{jk} + a\delta_{jk}$ using equation (1.15). Therefore, the only non-vanishing component for a cylindrically symmetric force distribution is

$$\kappa = \tilde{\mathsf{S}}_{33} = 3a, \tag{1.28}$$

where a is given by equation (1.21). The stresslet velocity field may be then written as

$$\boldsymbol{u}^D(\boldsymbol{r}, \hat{\boldsymbol{e}}_z) = -\tilde{\mathsf{S}}_{jk}\mathcal{G}_{ijk}\hat{\boldsymbol{e}}_i = -\kappa\ \partial_z \mathcal{G}_{i3}\hat{\boldsymbol{e}}_i \tag{1.29}$$

$$= -\kappa\ \partial_z \boldsymbol{u}^S(\boldsymbol{r}, \hat{\boldsymbol{e}}_z). \tag{1.30}$$

This concludes the derivation of the dipolar flow field due to an axisymmetric swimmer, quoted in equation (2.4) of the main text.

1.3.4. *Quadrupolar contribution*

Using the identity from equation (1.17) we rewrite the quadrupole moment tensor as $\tilde{\mathsf{Q}}_{jkl} = \mathsf{Q}_{jkl} - \frac{1}{4}\mathsf{Q}_{\alpha\alpha l}\delta_{jk} - \frac{1}{4}\mathsf{Q}_{\alpha k\alpha l}\delta_{jl}$, so that $\tilde{\mathsf{Q}}_{\alpha\alpha l} = \tilde{\mathsf{Q}}_{\alpha l\alpha} = 0$ and $\tilde{\mathsf{Q}}_{jkl}\mathcal{G}_{ijkl} = \mathsf{Q}_{jkl}\mathcal{G}_{ijkl}$. Evaluating $\tilde{\mathsf{Q}}_{jkl}$ by substituting equations (1.12) - (1.13) into the definition for Q_{jkl}, given in equation (1.10), and using equation (1.14) to integrate over the ϕ co-ordinate gives three independent coefficients

$$c = 2\pi \int \frac{1}{4} z(z f_z - \rho f_\rho) J dz, \tag{1.31}$$

$$d = 2\pi \int \frac{1}{2} z \rho f_\phi J dz, \tag{1.32}$$

$$e = 2\pi \int \frac{1}{2} \rho^2 f_z J dz. \tag{1.33}$$

We can then rewrite the tensor once more as $\tilde{\tilde{\mathsf{Q}}}_{jkl} = \tilde{\mathsf{Q}}_{jkl} + c\delta_{jk}\delta_{l3} + c\delta_{jl}\delta_{k3}$ so that

$$\tilde{\tilde{\mathsf{Q}}}_{jkl} = \begin{pmatrix} (0,0,0) & (0,0,Q_r) & (0,Q_r,0) \\ (0,0,-Q_r) & (0,0,0) & (-Q_r,0,0) \\ (-Q_\perp,0,0) & (0,-Q_\perp,0) & (0,0,-Q_\parallel) \end{pmatrix}, \tag{1.34}$$

where

$$Q_\parallel = -4c, \qquad Q_\perp = -e, \qquad Q_r = -d. \tag{1.35}$$

Hence, the quadrupolar velocity field due to an axisymmetric swimmer is

$$\boldsymbol{u}^Q(\boldsymbol{r}, \hat{\boldsymbol{e}}_z) = \frac{1}{2}\tilde{\tilde{\mathsf{Q}}}_{jkl}\mathcal{G}_{ijkl}\hat{\boldsymbol{e}}_i \tag{1.36}$$

$$= -\frac{1}{2}\left[Q_\parallel \partial_z^2 \boldsymbol{u}_z^S + Q_\perp(\partial_x^2 + \partial_y^2)\boldsymbol{u}_z^S\right] + Q_r \partial_z(\partial_y \boldsymbol{u}_x^S - \partial_x \boldsymbol{u}_y^S). \tag{1.37}$$

In order to write the expression in a form that is independent of the choice of coordinate system, we use the identity from equation (1.26) to give

$$\partial_y \boldsymbol{u}_x^S - \partial_x \boldsymbol{u}_y^S = \varepsilon_{zjk}\mathcal{G}_{ijk} = \varepsilon_{ikj}\mathcal{G}_{jzk} = (\boldsymbol{\nabla} \times \boldsymbol{u}_z^S)_i. \tag{1.38}$$

We also define $\nabla_\parallel^2 = (\hat{\boldsymbol{e}}_z \cdot \boldsymbol{\nabla})^2$ and $\nabla_\perp^2 = \nabla^2 - \nabla_\parallel^2$ as the Laplace operators parallel to, and in the plane perpendicular to, the swimming direction $\hat{\boldsymbol{e}}_z$. Inserting these into equation (1.37) yields

$$\boldsymbol{u}^Q(\boldsymbol{r}, \hat{\boldsymbol{e}}_z) = -\frac{1}{2}\left(Q_\parallel \nabla_\parallel^2 + Q_\perp \nabla_\perp^2 - 2Q_r \partial_z \boldsymbol{\nabla}\times\right)\boldsymbol{u}^S(\boldsymbol{r}, \hat{\boldsymbol{e}}_z). \tag{1.39}$$

This concludes the derivation of the quadrupolar flow field, quoted in equation (2.5) of the main text. However, this expression can be rewritten a bit further so that it will be easier to integrate later on. Notice that the Laplacian of the Stokeslet can be written as

$$\nabla^2 \boldsymbol{u}^S(\boldsymbol{r}, \hat{\boldsymbol{e}}_z) = -2(\hat{\boldsymbol{e}}_z \cdot \boldsymbol{\nabla})\boldsymbol{\nabla}\left(\frac{1}{r}\right), \tag{1.40}$$

which follows directly from inserting the Stokeslet velocity field (1.3) and pressure field (1.5) into Stokes' equations (1.1). Therefore, equation (1.39) can be written in terms of a derivative in the swimming direction:

$$\boldsymbol{u}^Q(\boldsymbol{r}, \hat{\boldsymbol{e}}_z) = \partial_z \left[Q_\perp \boldsymbol{\nabla}\left(\frac{1}{r}\right) + \frac{Q_\perp - Q_\parallel}{2} \partial_z \boldsymbol{u}^S(\boldsymbol{r}, \hat{\boldsymbol{e}}_z) + Q_r \boldsymbol{\nabla} \times \boldsymbol{u}^S(\boldsymbol{r}, \hat{\boldsymbol{e}}_z) \right]. \tag{1.41}$$

It will be useful to note that a particular combination of the quadrupole terms,

$$\boldsymbol{s}^D(\boldsymbol{r}, \hat{\boldsymbol{e}}_z) = \boldsymbol{u}^Q(\boldsymbol{r}, \hat{\boldsymbol{e}}_z \ ; \ Q_{sd} = Q_\parallel = Q_\perp, \ Q_r = 0) \tag{1.42}$$

$$= Q_{sd} \ \partial_z \boldsymbol{\nabla}\left(\frac{1}{r}\right), \tag{1.43}$$

corresponds to the source doublet flow field, where Q_{sd} is the source doublet strength. Similarly,

$$\boldsymbol{r}^D(\boldsymbol{r}, \hat{\boldsymbol{e}}_z) = \boldsymbol{u}^Q(\boldsymbol{r}, \hat{\boldsymbol{e}}_z \ ; \ Q_\parallel = Q_\perp = 0, \ Q_r) \tag{1.44}$$

$$= Q_r \ \partial_z \boldsymbol{\nabla} \times \boldsymbol{u}^S(\boldsymbol{r}, \hat{\boldsymbol{e}}_z) \tag{1.45}$$

corresponds to the rotlet doublet flow field, where Q_r is the rotlet doublet strength.

1.3.5. *Octupolar contribution*

Using the same method as in § 1.3.4 we find three independent components

$$O_\parallel = 2\pi \int \frac{1}{2} z^2 (2z f_z - 3\rho f_\rho) J dz, \tag{1.46}$$

$$O_\perp = 2\pi \int \frac{1}{8} \rho^2 (4z f_z - \rho f_\rho) J dz, \tag{1.47}$$

$$O_r = 2\pi \int \frac{1}{8} \rho (\rho^2 - 4z^2) f_\phi J dz. \tag{1.48}$$

Hence, we obtain the octupolar flow field

$$\boldsymbol{u}^O(\boldsymbol{r}, \hat{\boldsymbol{e}}_z) = -\frac{1}{6} \tilde{\mathcal{O}}_{jkl} \mathcal{G}_{ijklm} \hat{\boldsymbol{e}}_i = -\frac{1}{6} \left(O_\parallel \partial_z^3 + O_\perp (3\partial_z \partial_x^2 + 3\partial_z \partial_y^2) \right) \boldsymbol{u}^S(\boldsymbol{r}, \hat{\boldsymbol{e}}_z)$$
$$- \frac{O_r}{6} \left(3\partial_y \partial_z^2 \boldsymbol{u}^S(\boldsymbol{r}, \hat{\boldsymbol{e}}_x) - 3\partial_x \partial_z^2 \boldsymbol{u}^S(\boldsymbol{r}, \hat{\boldsymbol{e}}_y) \right), \tag{1.49}$$

which may be rewritten using equation (1.38) to give the octupolar flow field due to an axisymmetric swimmer

$$\boldsymbol{u}^O(\boldsymbol{r}, \hat{\boldsymbol{e}}_z) = -(\hat{\boldsymbol{e}}_z \cdot \boldsymbol{\nabla}) \left[\frac{O_\parallel}{6} \nabla_\parallel^2 + \frac{O_\perp}{2} \nabla_\perp^2 + \frac{O_r}{2} (\hat{\boldsymbol{e}}_z \cdot \boldsymbol{\nabla}) \boldsymbol{\nabla} \times \right] \boldsymbol{u}^S(\boldsymbol{r}, \hat{\boldsymbol{e}}_z). \tag{1.50}$$

1.3.6. *Higher order contributions*

We finish this section by noting that higher order contributions to the flow field can be derived in exactly the same fashion. For an axisymmetric micro-swimmer each order

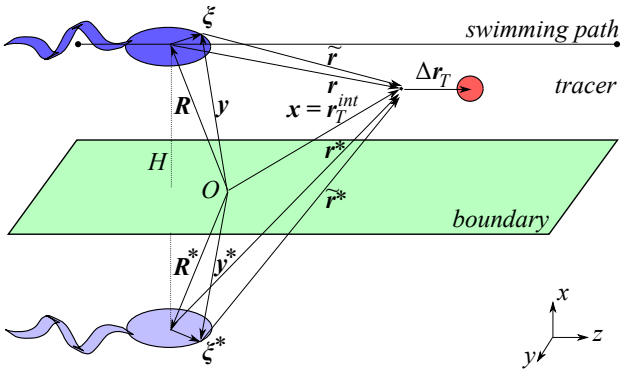

Figure 3: Geometry diagram for a micro-swimmer moving along a path parallel to a boundary. The unit vector normal to the boundary is $\hat{\boldsymbol{n}} = \hat{\boldsymbol{e}}_x$ and the swimmer moves at a distance H from the boundary with velocity V in the z-direction. Note that the axes are displayed in the bottom-right corner, not at the origin, for clarity.

has three independent coefficients, analogous to $Q_{\parallel,\perp,r}$ and $O_{\parallel,\perp,r}$. The hexadecapolar flow field can then be written as

$$\boldsymbol{u}^H(\boldsymbol{r},\hat{\boldsymbol{e}}_z) = -(\hat{\boldsymbol{e}}_z\cdot\boldsymbol{\nabla})^2\frac{1}{4!}\left[H_\parallel\nabla_\parallel^2 + 3H_\perp\nabla_\perp^2 + 4H_r(\hat{\boldsymbol{e}}_z\cdot\boldsymbol{\nabla})\boldsymbol{\nabla}\times\right]\boldsymbol{u}^S(\boldsymbol{r},\hat{\boldsymbol{e}}_z), \quad (1.51)$$

and similarly for higher orders, with increasingly higher powers of $(\hat{\boldsymbol{e}}_z\cdot\boldsymbol{\nabla})$. Figure 2 shows a pictorial summary of the lower order multipoles.

2. Mathematical model: flow field in a semi-infinite fluid

Close to a no-slip or free-slip boundary, the confinement affects the flow field as it introduces extra boundary conditions to the solutions of the Stokes equations (1.1). For a free-slip surface such as a liquid-air interface there is a no-penetration condition, $\boldsymbol{u}\cdot\hat{\boldsymbol{n}} = 0$, where $\hat{\boldsymbol{n}}$ is a unit vector normal to the surface. Additionally, there is a no-shear condition, $\mathsf{E} = \frac{1}{2}(\nabla\boldsymbol{u} + (\nabla\boldsymbol{u})^T) = 0$, at the interface with an inviscid fluid. For liquid-solid boundaries there is a no-slip boundary condition, $\boldsymbol{u} = 0$, at the interface. These boundary conditions can be satisfied by the method of images.

Consider an infinite and flat boundary in the plane $x = 0$ so that $\hat{\boldsymbol{n}} = \hat{\boldsymbol{e}}_x$. A micro-swimmer is located at position $\boldsymbol{R}$, a distance H from the boundary. Its surface, where forces are exerted onto the fluid, is located at $\boldsymbol{y} = \boldsymbol{R} + \boldsymbol{\xi}$, a distance $\tilde{H}$ from the boundary. For the image system, denoted by the asterix, we define the mirror matrix $\mathsf{M} = \mathrm{diag}(-1,1,1)$. The image swimmer is then located at position $\boldsymbol{R}^* = \mathsf{M}\boldsymbol{R}$ with its surface located at $\boldsymbol{y}^* = \mathsf{M}\boldsymbol{y} = \boldsymbol{R}^* + \boldsymbol{\xi}^*$. The relative position variables of the swimmer's body centre and surface with respect to a point $\boldsymbol{x}$ in the fluid are defined as $\boldsymbol{r}^{(*)} = \boldsymbol{x} - \boldsymbol{R}^{(*)}$ and $\tilde{\boldsymbol{r}}^{(*)} = \boldsymbol{x} - \boldsymbol{y}^{(*)}$ respectively. This geometry is shown in figure 3.

2.1. *Image system for a free-slip boundary*

As in § 1.1, we consider a point force $\boldsymbol{F}^S(\boldsymbol{x},\boldsymbol{y}) = \delta^3(\boldsymbol{x}-\boldsymbol{y})\boldsymbol{f}^S$ acting at the point $\boldsymbol{y}$ on the surface of the swimmer, where $\boldsymbol{f}^S$ is the force strength. The Stokeslet, the flow field $\boldsymbol{u}^S$ generated at the point $\boldsymbol{x}$ by the point force $\boldsymbol{F}^S$, is given by equation (1.3). The flow

field of the image system is

$$u_i^{S*}(\boldsymbol{x},\boldsymbol{y}^*;\boldsymbol{f}^S) = f_j^S \cdot \mathcal{F}_{ij}(\tilde{\boldsymbol{r}}^* = \boldsymbol{x}-\boldsymbol{y}^*), \tag{2.1}$$

$$\mathcal{F}_{ij}(\boldsymbol{r}) = M_{jk}\mathcal{G}_{ik}(\boldsymbol{r}) = \frac{1}{8\pi\mu}M_{jk}\left(\frac{\delta_{ik}}{r}+\frac{r_i r_k}{r^3}\right), \tag{2.2}$$

where the Green's function $\mathcal{F}_{ij}$ does not depend explicitly on H.

2.2. *Image system for a no-slip boundary*

For the case of a no-slip boundary, the image system is more complicated because all three components of the velocity field must vanish at the boundary. The solution was derived first by Lorentz using a reciprocal theorem method by Lorentz (1896). Later it was rederived by Blake (1971) using a Fourier transform approach that yields a more intuitive solution in the form of a Green's function, so that the velocity field can be written in the form of equation (2.1). This Green's function, often called the Blake tensor, is

$$\mathcal{B}_{ij}(\boldsymbol{x},\boldsymbol{r}^*) = \frac{1}{8\pi\mu}\left[-\left(\frac{\delta_{ij}}{r^*}+\frac{r_i^* r_j^*}{r^{*3}}\right)+2HM_{jl}\frac{\partial}{\partial r_l^*}\left(\frac{Hr_i^*}{r^{*3}}-\left(\frac{\delta_{ix}}{r^*}+\frac{r_i^* r_x^*}{r^{*3}}\right)\right)\right], \tag{2.3}$$

where $H = (\boldsymbol{r}^* - \boldsymbol{x})\cdot\hat{\boldsymbol{e}}_x > 0$. For a Stokeslet oriented parallel (perpendicular) to the boundary this image system can be decomposed into three parts. The first part is a Stokeslet of equal magnitude f but pointing in the opposite direction. The second is an asymmetric dipole, sometimes called the Stokes doublet (symmetric dipole $\boldsymbol{u}^D$), with magnitude D_{13} (D_{11}) equal to $2Hf$. The third part is quadrupolar, being a source doublet $\boldsymbol{s}^D$ oriented in the opposite (same) direction with magnitude $Q_{sd} = 2H^2 f$. Hence, the Blake tensor can be rewritten as

$$\mathcal{B}_{ij}(\boldsymbol{x},\boldsymbol{r}^*) = \left(-\mathcal{G}_{ij}(\boldsymbol{r}) - 2HM_{jk}\frac{\partial\mathcal{G}_{iz}(\boldsymbol{r})}{\partial r_k} + H^2 M_{jk}\nabla^2\mathcal{G}_{ik}(\boldsymbol{r})\right)\Big|_{\boldsymbol{r}=\boldsymbol{r}^*} \tag{2.4}$$

$$= (-\delta_{jk} - 2H\delta_{kx}\partial_j + H^2 M_{jk}\nabla^2)\mathcal{G}_{ik}(\boldsymbol{r}^*), \tag{2.5}$$

where the derivatives $\partial_j^* = M_{jl}\partial_l$ and $\nabla^{*2} = \nabla^2$.

2.3. *Multipole expansion in a semi-infinite fluid*

As in § 1.2, we model the swimmer's flow field as being generated by a distribution of point forces $\boldsymbol{f}(\boldsymbol{\xi})$, each with its Stokeslet solution $\mathcal{G}_{ij}$ and its appropriate image system $\mathcal{F}_{ij}$ or $\mathcal{B}_{ij}$, integrated over the swimmer's surface $S(\boldsymbol{\xi})$. The velocity field is then given by

$$u_i^{sw+im}(\boldsymbol{r}) = \int_S \Big\{\mathcal{G}_{ij}(\boldsymbol{r}-\boldsymbol{\xi}) + \mathcal{B}_{ij}(\boldsymbol{r}^*-\boldsymbol{\xi}^*)\Big\} f_j(\boldsymbol{\xi})dS. \tag{2.6}$$

Exactly as in § 1.2 we perform a multipole expansion, considering the Stokeslet and image system separately for small $\boldsymbol{\xi}$ and $\boldsymbol{\xi}^* = M\boldsymbol{\xi}$ values. For the first term in equation (2.6), we expand the Oseen tensor in small values of $\boldsymbol{\xi}$ around the relative position $\boldsymbol{r}$. The result is given in equation (1.7). For the image term, we expand the Blake tensor in small values of $\boldsymbol{\xi}^* = M\boldsymbol{\xi}$ around $\boldsymbol{r}^*$ which yields

$$u_i^{im}(\boldsymbol{r}^*) = \int_S \left[\mathcal{B}_{ij}(\boldsymbol{r}^*) - \frac{\partial\mathcal{B}_{ij}(\boldsymbol{r}^*)}{\partial r_k^*}\xi_k^* + \frac{1}{2}\frac{\partial^2\mathcal{B}_{ij}(\boldsymbol{r}^*)}{\partial r_k^*\partial r_l^*}\xi_k^*\xi_l^* + \ldots\right] f_j(\boldsymbol{\xi})dS. \tag{2.7}$$

We rewrite this in terms of $\boldsymbol{\xi}$, noting that $\xi_j^* = M_{jk}\xi_k$ and $(\partial r_k/\partial r_j^*) = M_{jk}$. Hence, taking the expressions independent of $\boldsymbol{\xi}$ out of the integrals yields

$$u_i^{im}(\boldsymbol{r}) = \mathcal{B}_{ij}\int_S f_j dS - \frac{\partial\mathcal{B}_{ij}}{\partial r_k}\int_S f_j\xi_k dS + \frac{1}{2}\frac{\partial^2\mathcal{B}_{ij}}{\partial r_k\partial r_l}\int_S f_j\xi_k\xi_l dS + \ldots \tag{2.8}$$

$$= \mathcal{B}_{ij}\mathsf{F}_j - \mathcal{B}_{ijk}\mathsf{D}_{jk} + \frac{1}{2}\mathcal{B}_{ijkl}\mathsf{Q}_{jkl} - \frac{1}{3!}\mathcal{B}_{ijklm}\mathsf{O}_{jklm} + \dots, \tag{2.9}$$

where care has to be taken when evaluating the derivatives, to take into account the full dependence of $\mathcal{B}(\boldsymbol{r}^*)$ on $\boldsymbol{r}$. For a free-slip boundary, $\mathcal{B}$ is simply replaced with $\mathcal{F}$.

Comparing equations (2.8)-(2.9) with equations (1.7)-(1.9) we see that they take an identical form with the same prefactors, the force strength F_i, the dipole strength D_{ij}, and so on. Because the swimmer is still free of net external forces or torques, we can keep the same parameters $\kappa, Q_{\parallel,\perp,r}, \dots$ derived in § 1.3 for a cylindrically symmetric swimmer.

2.4. *Effective Stokeslets*

Using these simplifications, we note that as the flow field $\boldsymbol{u}^{sw}(\boldsymbol{r}, \hat{\boldsymbol{e}}_k)$ for a micro-swimmer moving in the $\hat{\boldsymbol{e}}_k$ direction takes the form of equation (1.11), the image flow field can be written in the similar form

$$\boldsymbol{u}^{im}(\boldsymbol{r}, \hat{\boldsymbol{e}}_k) = \boldsymbol{u}^{D*}(\boldsymbol{r}, \hat{\boldsymbol{e}}_k; \kappa) + \boldsymbol{u}^{Q*}(\boldsymbol{r}, \hat{\boldsymbol{e}}_k; Q_{\parallel,\perp,r}) + \dots, \tag{2.10}$$

so that the total velocity field $\boldsymbol{u}^{sw+im}$ is given by adding equations (1.11) and (2.10).

To evaluate this we define the three effective Stokeslets

$$\overline{\boldsymbol{u}}^S(\boldsymbol{r}, \hat{\boldsymbol{e}}_j) = \hat{\boldsymbol{e}}_j \cdot (\mathcal{G}_{ij} + \mathcal{B}_{ij}) \tag{2.11}$$

in the three directions $j \in \{x, y, z\}$. The velocity fields including the boundary effects are then given by replacing the Stokeslets $\boldsymbol{u}_j^S$ with the effective Stokeslets $\overline{\boldsymbol{u}}_j^S$, where we have used the short-hand notation $\boldsymbol{u}_j^S = \boldsymbol{u}^S(\boldsymbol{r}, \hat{\boldsymbol{e}}_j)$. Particularly, the dipolar and quadrupolar flow fields, given in equations (1.30) and (1.39) respectively, can be written as

$$\boldsymbol{u}^{sw+im}(\boldsymbol{r}, \hat{\boldsymbol{e}}_k) = \left(-\kappa\partial_z - \frac{1}{2}Q_\parallel\nabla_\parallel^2 - \frac{1}{2}Q_\perp\nabla_\perp^2 + Q_r\partial_z\boldsymbol{\nabla}\times\right)\overline{\boldsymbol{u}}^S(\boldsymbol{r}, \hat{\boldsymbol{e}}_k). \tag{2.12}$$

In the next two sections this will be written out explicity and described for the cases of a free-slip boundary and a no-slip boundary respectively.

2.5. *Flow field for a free-slip boundary*

The effective Stokeslets for a free-slip boundary are

$$\overline{\boldsymbol{u}}_j^S = \hat{\boldsymbol{e}}_j \cdot (\mathcal{G}_{ij} + \mathcal{F}_{ij}) = \boldsymbol{u}_j^S + \mathsf{M}_{jk}\boldsymbol{u}_k^{S*}, \tag{2.13}$$

where the image Stokelet $\boldsymbol{u}^{S*}(\boldsymbol{r}, \hat{\boldsymbol{e}}_j) = \boldsymbol{u}_j^S(\boldsymbol{r}^*, \hat{\boldsymbol{e}}_j)$.

Substituting $\overline{\boldsymbol{u}}_z^S$ into equation (2.12) for a swimmer moving along $\hat{\boldsymbol{e}}_z$, parallel to a free-slip boundary, and rewriting the resulting expression with the derivatives in the swimming direction $\partial_z = \partial_z^*$ moved out of the brackets gives

$$\begin{aligned}\boldsymbol{u}^{sw+im}(\boldsymbol{r}, \hat{\boldsymbol{e}}_z) = {}& \partial_z\left[-\kappa\boldsymbol{u}_z^S + Q_\perp\boldsymbol{\nabla}\left(\frac{1}{r}\right) + \frac{Q_\parallel - Q_\perp}{2}\partial_z\boldsymbol{u}_z^S + Q_r\boldsymbol{\nabla}\times\boldsymbol{u}_z^S\right] \\ & + \partial_z^*\left[-\kappa\boldsymbol{u}_z^{S*} + Q_\perp\boldsymbol{\nabla}^*\left(\frac{1}{r^*}\right) + \frac{Q_\parallel - Q_\perp}{2}\partial_z^*\boldsymbol{u}_z^{S*} - Q_r\boldsymbol{\nabla}^*\times\boldsymbol{u}_z^{S*}\right] \\ & + O(r^{-4}).\end{aligned} \tag{2.14}$$

Notice that in this form the swimmer and image contributions are kept separate, and written in terms of their coordinates $\boldsymbol{r}$ and $\boldsymbol{r}^*$ respectively. The contributions are identical except for their position in space and the minus sign of the last term proportional to Q_r in equation (2.14). Since this term models the rotation of the head and tail (*i.e.* in the negative and positive angular directions respectively), the minus sign indicates that

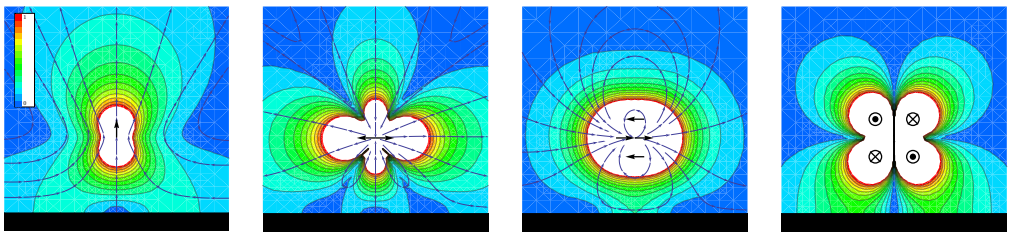

(a) Stokeslet $f_z = 1$ (b) Dipole $\kappa = 1$ (c) Source doublet $Q_\parallel = 1, Q_\perp = 1$ (d) Rotlet doublet $Q_r = 1$

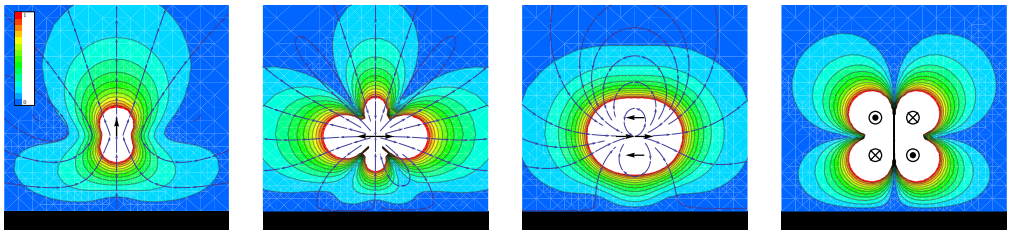

(e) Stokeslet $f_z = 1$ (f) Dipole $\kappa = 1$ (g) Source doublet $Q_\parallel = 1, Q_\perp = 1$ (h) Rotlet doublet $Q_r = 1$

Figure 4: Flow fields produced by a swimmer moving parallel to (*a-d*) a free-slip boundary, (*e-h*) a no-slip boundary, as seen in the (z, x) plane in the laboratory frame. Arrows indicate the velocity direction, colours portray its relative magnitude ranging from zero (blue) to unity (red) and white denotes the singularity center.

the image head and tail rotate in the opposite directions. Therfore, it becomes apparent that the image system is an identical but mirrored swimmer. The resulting flow fields due to the lower order multipoles are portrayed in figures 4a - 4d. Notice in particular that the magnitude of the flow is increased near the boundary by cooperation between the swimmer and image.

2.6. *Flow field for a no-slip boundary*

The effective Stokelets for a no-slip boundary, using equation (2.5), are

$$\overline{\boldsymbol{u}}_j^S = \boldsymbol{u}_j^S - \boldsymbol{u}_j^{S*} - 2H M_{jk} \partial_k^* \boldsymbol{u}_x^{S*} + H^2 \nabla^2 M_{jk} \boldsymbol{u}_k^{S*}. \tag{2.15}$$

As in § 2.5, we substitute $\overline{\boldsymbol{u}}_z^S$ from equation (2.15) into equation (2.12) for a swimmer moving parallel to a no-slip boundary and rewrite the resulting expression as a differential of ∂_z.

$$\begin{aligned}\boldsymbol{u}^{sw+im}(\boldsymbol{r}; \hat{\boldsymbol{e}}_z) = \partial_z \Bigg[&- \kappa \overline{\boldsymbol{u}}_z^S + Q_\perp \left\{ \boldsymbol{\nabla} \left(\frac{1}{r} \right) + \left(-1 - 2H\partial_x^* + H^2 \boldsymbol{\nabla}^{*2} \right) \boldsymbol{\nabla}^* \left(\frac{1}{r^*} \right) \right\} \\ &+ \frac{Q_\parallel - Q_\perp}{2} \partial_z \overline{\boldsymbol{u}}_z^S + Q_r (\partial_y \overline{\boldsymbol{u}}_x^S - \partial_x \overline{\boldsymbol{u}}_y^S) \Bigg] + O(r^{-4}). \end{aligned} \tag{2.16}$$

The structure of the image system is not immediately evident from this expression. For example, the image system of a pusher dipole can be decomposed into a puller dipole, a quadrupolar $Q_\perp$ term oriented in the $-z$ direction, and an octupolar term.

The resulting flow fields are portrayed in figures 4e - 4h. Close to the swimmer the velocity tends to that of a swimmer in an infinite fluid, as shown in figure 2. Image effects are seen at the boundary, where the velocity field vanishes as required, and in the far-field, where the distance to the swimmer and image is again comparable. This can lead to

interesting effects. For the source doublet swimmer shown in figure 4g for example, the flow in the z direction is enhanced between the boundary and the swimmer, compared to a swimmer in an infinite fluid, despite the no-slip condition.

3. Computing the separatrix

3.1. *The flow field stream function*

We showed that the flow field generated by a cylindrically symmetric micro-swimmer can be written in terms of a multipole expansion (1.9), and in § 1.3 we gave expressions for these terms up to octupolar order. This flow field may be written in terms of a stream function (Pushkin *et al.* 2013).

We define the stream function $\psi(z,\rho)$ in the reference frame co-moving with the swimmer with speed $V \geqslant 0$ in the z direction, where the swimmer is located at the origin. The radial and longitudinal components of the swimmer's flow field are then given by

$$\frac{\partial \psi}{\partial \rho} = -2\pi\rho u_z^{sw}(z,\rho), \quad \frac{\partial \psi}{\partial z} = 2\pi\rho u_\rho^{sw}(z,\rho), \tag{3.1}$$

where r is the distance from the swimmer, $z = r\cos\theta$, $\rho = r\sin\theta$. Note that the azimuthal components of the flow field do not depend on the stream function, so the terms due to the rotation of the flagella and head of the swimmer do not enter this derivation.

Substituting the swimmer flow field, where the dipolar, quadrupolar, octupolar terms are given by equations (1.30), (1.39) and (1.50) respectively, into equation (3.1) and integrating gives

$$\begin{aligned}\psi(z,\rho) = \; & 2\pi\rho^2\left[\frac{V}{2} - \frac{\kappa\cos\theta}{r^2} - \left(Q_\parallel \frac{1-\cos^2\theta}{2} + Q_\perp \frac{1+\cos^2\theta}{2}\right)\frac{1}{r^3}\right. \\ & \left. + \left(O_\parallel \frac{3\cos\theta - 5\cos^3\theta}{2} + O_\perp \frac{-3\cos\theta + 15\cos^3\theta}{2}\right)\frac{1}{r^4}\right] + O\left(\frac{1}{r^5}\right). \end{aligned} \tag{3.2}$$

The additive constant of integration is chosen so that the influence of the swimmer vanishes as $r \to \infty$.

3.2. *Definition of the separatrix*

The level curves of the stream function, given by $\psi(r,\theta) = C$, a constant, form a surface of streamlines, enclosing a streamtube. The volume flux going through this streamtube is equal to C, due to the convenient choice of additive constant.

We aim to find a surface around the swimmer through which no fluid passes so that the flow is separated into two regions: an internal one containg the swimmer singularities and an external region that is singularity-free. Consquently, the swimmer can be attributed with an effective finite size given by the volume enclosed by the separating surface.

This separatrix, defined by $r = \Sigma(\theta)$ with r finite and positive for all values of θ, particularly at $\theta = 0, \pi$, is given by the streamtube with zero volume flux going through it, which connects two stagnation points on the z-axis in front of and behind the swimmer. Hence, we must solve $\psi(r,\theta) = 0$ for $r = \Sigma(\theta)$, where ψ is given by equation (3.2). If terms up to octupolar order are considered in the stream function, this requires finding the roots of a quartic equation, which can be done analytically. We will evaluate the solution for several cases in the following sections.

3.3. *Solution for a quadrupolar swimmer*

First we consider the simple case of a pure quadrupolar swimmer, so that $\kappa = 0$ and $O_\parallel = O_\perp = 0$. Equation (3.2) then immediately gives a single real root

$$\Sigma_Q(\theta) = \left(\frac{Q_\parallel(1 - 3\cos^2\theta) + Q_\perp(1 + 3\cos^2\theta)}{V} \right)^{1/3}. \tag{3.3}$$

This root is positive for all values of θ if

$$Q_\perp > 0, \qquad -1 < Q_\parallel/Q_\perp < 2. \tag{3.4}$$

If these conditions hold the separatrix around the quadrupolar micro-swimmer exists. In particular, for a swimmer with a flow field that is a pure source doublet, such that $Q_\parallel = Q_\perp = Q_{sd}$, we find that the separatrix is a spherical shell with constant radius

$$a_{sw} = \left(\frac{2Q_{sd}}{V} \right)^{1/3}. \tag{3.5}$$

This result is shown in figure 2b of the main text.

3.4. *Solution for a swimmer with dipolar plus quadrupolar flow field.*

We extend the solution to account for a model swimmer that also has a dipolar contribution to its flow field, so that $\kappa \neq 0$. So we look for the roots of the equation $0 = r^3 + pr + q$, where

$$p = -\frac{2\kappa\cos\theta}{V}, \quad q = -\frac{Q_\parallel(1 - 3\cos^2\theta) + Q_\perp(1 + 3\cos^2\theta)}{V}. \tag{3.6}$$

The three solutions r_k are

$$r_k = -\frac{u_k}{3}\left(\frac{27q + \sqrt{27^2q^2 + 4\ 27p^3}}{2} \right)^{1/3} + \frac{p}{u_k}\left(\frac{27q + \sqrt{27^2q^2 + 4\ 27p^3}}{2} \right)^{-1/3}, \tag{3.7}$$

$$u_1 = 1, \quad u_2 = \frac{-1 + i\sqrt{3}}{2}, \quad u_3 = \frac{-1 - i\sqrt{3}}{2}. \tag{3.8}$$

The discriminant of this cubic equation is $\Delta = -4p^3 - 27q^2$. There is only one real solution to the cubic equation if $\Delta < 0$. This is the case for all values of θ if $|8\kappa^3| < 27(Q_\parallel - 2Q_\perp)^2 V$, and in this case the solution r_1 is positive if the conditions (3.4) are satisfied. If $\Delta > 0$ there are three real solutions to the cubic equation. If $|8\kappa^3| > 27(Q_\parallel - 2Q_\perp)^2 V$ this will be the case for a range of θ values. Nevertheless, if the conditions (3.4) are satisfied then the first solution r_1 will be real and positive for all values of θ. The other two solutions r_2 and r_3 will be negative and need not be considered as physical solutions.

Hence, if the conditions (3.4) hold, we have the physical solution

$$\Sigma_\kappa(\theta) = r_1, \tag{3.9}$$

for all values of κ. This solution corresponds to the surface formed by the streamlines connecting two stagnation points located on the z-axis in front of and behind the swimmer, with z positions given by $u_z^{sw}(\rho = 0, z^*) - V = 0$. Examples of this solution are shown in figures 2c and 2d of the main text.

4. Integrating the tracer equations of motion

In § 3 of the main text we showed that after expanding the tracer equation of motion

$$\frac{d\boldsymbol{r}_T}{dt} = \boldsymbol{u}^{sw}\left(\boldsymbol{r}_T - \boldsymbol{R}; \hat{\boldsymbol{e}}_z\right) + \boldsymbol{u}^{im}\left(\boldsymbol{r}_T - \boldsymbol{R}^*; \hat{\boldsymbol{e}}_z\right), \tag{4.1}$$

the tracer trajectory can be written as

$$\boldsymbol{\Delta r}_T(t) = \Delta \boldsymbol{r}_T^{(1)} + \Delta \boldsymbol{r}_T^{(2)} + \Delta \boldsymbol{r}_T^{(3)} + \dots, \tag{4.2}$$

where the terms $\Delta \boldsymbol{r}_T^{(n)}$ of this perturbative expansion can be found by integrating the succesive equations of motion MT(2.11)-(2.14). The initial conditions are $\Delta \boldsymbol{r}_T^{int(n)} = \boldsymbol{0}$ for all n, and without loss of generality we set $z_T^{int} = 0$.

4.1. *Micro-swimmer in an unbounded fluid*

We begin with the leading term, given by equation MT(2.11), into which we substitute the dipolar flow field given by equation MT(2.4). Note that integrating over time t is equivalent to integrating over the swimmer position $R_z = R_z^{int} + Vt$. Therefore, $(\hat{\boldsymbol{e}}_z \cdot \boldsymbol{\nabla}) = \partial_z = -V^{-1}\partial_t$ and hence we find the perfect differential

$$\frac{d\boldsymbol{\Delta r}_T^{(1)}}{dt} = \boldsymbol{u}^D = -\frac{1}{V}\frac{d}{dt}\left[-\kappa\, \boldsymbol{u}^S\right]. \tag{4.3}$$

Hence, direct integration yields the leading order contributions to the tracer trajectory as a function of the swimmer position, or equivalently of time $t = (R_z - R_z^{int})/V$,

$$\boldsymbol{\Delta r}_T^{(1)}(R_z) = V^{-1}\left[\kappa\, \boldsymbol{u}^S\right]_{\boldsymbol{r}(R_z^{int})}^{\boldsymbol{r}(R_z)}. \tag{4.4}$$

Evaluating this explicitly in terms of the cylindrical polar co-ordinates gives

$$\boldsymbol{\Delta r}_T^{(1)}(R_z) = \left[\frac{\kappa}{V}\frac{r^2 + R_z^2}{r^3}\hat{\boldsymbol{e}}_z - \frac{\kappa}{V}\frac{\rho R_z}{r^3}\hat{\boldsymbol{e}}_\rho\right]_{R_z^{int}}^{R_z}, \tag{4.5}$$

where $r^2 = R_z^2 + \rho^2$. This expression, as expected, is of order r^{-1}.

The second order contribution to the tracer displacement is given by

$$\partial_t \boldsymbol{\Delta r}_T^{(2)} = \boldsymbol{u}^Q. \tag{4.6}$$

Substituting in the expression for $\boldsymbol{u}^Q$ from equation (1.39) and integrating gives

$$\boldsymbol{\Delta r}_T^{(2)}(R_z) = -V^{-1}\left[Q_\perp \boldsymbol{\nabla}\left(\frac{1}{r}\right) + \frac{Q_\perp - Q_\parallel}{2}\partial_z \boldsymbol{u}^S + Q_r \boldsymbol{\nabla}\times \boldsymbol{u}^S\right]_{\boldsymbol{r}(R_z^{int})}^{\boldsymbol{r}(R_z)}. \tag{4.7}$$

$$= \left[\frac{2R_z^3(Q_\parallel - 2Q_\perp) - (Q_\parallel + Q_\perp)R_z\rho^2}{2Vr^5}\hat{\boldsymbol{e}}_z \right.$$
$$\left. - \frac{2\rho R_z^2(Q_\parallel - 2Q_\perp) - (Q_\parallel + Q_\perp)\rho^3}{2Vr^5}\hat{\boldsymbol{e}}_\rho - \frac{2Q_r}{V}\frac{\rho}{r^3}\hat{\boldsymbol{e}}_\phi\right]_{R_z^{int}}^{R_z}. \tag{4.8}$$

The third order contribution comes from the equation MT(2.13). Using equations (1.30) and (4.4) yields

$$\frac{d\boldsymbol{\Delta r}_T^{(3)}}{dt} = \boldsymbol{u}^O - \left(\frac{\kappa}{V}\boldsymbol{u}^S \cdot \boldsymbol{\nabla}\right)\kappa \partial_z \boldsymbol{u}^S. \tag{4.9}$$

The first term on the r.h.s., $\boldsymbol{u}^O$ given by equation (1.50), can again be written as a perfect

differential. This will be the case for all subsequent terms in the flow field $\boldsymbol{u}^H, \boldsymbol{u}^{32}, \ldots$. The second term is less trivial but can also be integrated analytically, giving

$$\begin{aligned}\boldsymbol{\Delta r}_T^{(3)}(R_z) = &\left[\frac{4(O_\parallel - 6O_\perp)R_z^4 + 2(-5O_\parallel + 12O_\perp)R_z^2\rho^2 + (O_\parallel + 3O_\perp)\rho^4}{6Vr^7}\hat{\boldsymbol{e}}_z\right.\\ &\left.-\frac{2(O_\parallel - 6O_\perp)R_z^3\rho + 3(O_\parallel - O_\perp)R_z\rho^3}{2Vr^7}\hat{\boldsymbol{e}}_\rho\frac{3O_r}{V}\frac{\rho R_z}{r^5}\hat{\boldsymbol{e}}_\phi\right]_{R_z^{int}}^{R_z}\\ +\frac{\kappa^2}{V^2}&\left[\frac{\rho(2\rho^2 - 5R_z^2)}{2r^6}\hat{\boldsymbol{e}}_\rho - \left(\frac{R_z(R_z^4 - 40R_z^2\rho^2 + 15\rho^4)}{16\rho^2r^6} + \frac{\arctan(R_z/\rho)}{16\rho^3}\right)\hat{\boldsymbol{e}}_z\right]_{R_z^{int}}^{R_z}.\end{aligned} \tag{4.10}$$

Notice that for infinite swimming paths, as the swimmer moves from $R_z = -\infty$ to ∞, the first and second order contributions to the tracer displacement given by equations (4.5) and (4.8) vanish. This does not mean the tracer trajectories themself vanish, but rather that they will form closed loops. Many terms in equation (4.10) drop out as well for large R_z values but, crucially, the term proportional to $\arctan(R_z/\rho)/\rho^3$ remains finite. The final tracer displacement is then given by

$$\boldsymbol{\Delta r}_T^{(3)} = \lim_{R_z\to+\infty}\boldsymbol{\Delta r}_T^{(3)}(R_z) - \lim_{R_z\to-\infty}\boldsymbol{\Delta r}_T^{(3)}(R_z) = -\frac{\pi\kappa^2}{16V^2}\frac{1}{\rho^3}\hat{\boldsymbol{e}}_z. \tag{4.11}$$

Therefore the third order contribution to the tracer displacement is the leading order term for infinite swimming paths.

The fourth order contribution to the tracer displacement stems from equation MT(2.14). Substituting in the flow fields given by equations (1.30) - (1.39) and the lower order contributions given by (4.4) - (4.7) yields

$$\begin{aligned}\frac{d\boldsymbol{\Delta r}_T^{(4)}}{dt} = \boldsymbol{u}^H &+ \left(\frac{\kappa}{V}\boldsymbol{u}^S\cdot\boldsymbol{\nabla}\right)\left(Q_\perp\partial_z\boldsymbol{\nabla}\left(\frac{1}{r}\right) + \frac{Q_\perp - Q_\parallel}{2}\partial_z^2\boldsymbol{u}^S + Q_r\partial_z(\boldsymbol{\nabla}\times\boldsymbol{u}^S)\right)\\ &+\left(\left(\frac{Q_\perp}{V}\boldsymbol{\nabla}\left(\frac{1}{r}\right) + \frac{Q_\perp - Q_\parallel}{2V}\partial_z\boldsymbol{u}^S + \frac{Q_r}{V}\boldsymbol{\nabla}\times\boldsymbol{u}^S\right)\cdot\boldsymbol{\nabla}\right)\kappa\partial_z\boldsymbol{u}^S.\end{aligned} \tag{4.12}$$

This expression can be integrated, but at this point we no longer write out the full fourth order contribution to the tracer trajectory for a finite swimming path because the first three contributions, given by equations (4.5), (4.8) and (4.10), dominate. Instead, we integrate the expression for an infinite swimming path giving

$$\boldsymbol{\Delta r}_T^{(4)} = \frac{9\pi\kappa Q_r}{8V^2}\frac{1}{\rho^4}\hat{\boldsymbol{e}}_\phi. \tag{4.13}$$

Notice that the terms proportional to $\kappa Q_\parallel$ and $\kappa Q_\perp$ vanish for an infinite swimming path. Hence, the fourth order contribution is purely azimuthal, as opposed to the third order, given by equation (4.11), which was purely longitudinal.

Higher order contributions can be calculated in exactly the same way. The fifth order

$$\begin{aligned}\partial_t\boldsymbol{\Delta r}_T^{(5)} = \boldsymbol{u}^{32} &+ \left(\boldsymbol{\Delta r}_T^{(3)}\cdot\boldsymbol{\nabla}\right)\boldsymbol{u}^D + \left(\boldsymbol{\Delta r}_T^{(2)}\cdot\boldsymbol{\nabla}\right)\boldsymbol{u}^Q + \left(\boldsymbol{\Delta r}_T^{(1)}\cdot\boldsymbol{\nabla}\right)\boldsymbol{u}^O\\ &+\frac{1}{2}\left(\boldsymbol{\Delta r}_T^{(1)}\cdot\boldsymbol{\nabla}\right)^2\boldsymbol{u}^D,\end{aligned} \tag{4.14}$$

which is integrated for an infinite swiming path to give

$$\boldsymbol{\Delta r}_T^{(5)} = \left(+\frac{9\pi(9Q_\parallel^2 + 14Q_\parallel Q_\perp + 41Q_\perp^2)}{1024V^2}\frac{1}{\rho^5} - \frac{9\pi\kappa(3O_\parallel + 7O_\perp)}{256V^2}\frac{1}{\rho^5}\right)\hat{\boldsymbol{e}}_z, \tag{4.15}$$

which is purely longitudinal as for $\boldsymbol{\Delta r}_T^{(3)}$.

Finally, the sixth order contribution

$$\partial_t \boldsymbol{\Delta r}_T^{(6)} = \boldsymbol{u}^{64} + \left(\boldsymbol{\Delta r}_T^{(4)} \cdot \boldsymbol{\nabla}\right) \boldsymbol{u}^D + \left(\boldsymbol{\Delta r}_T^{(3)} \cdot \boldsymbol{\nabla}\right) \boldsymbol{u}^Q + \left(\boldsymbol{\Delta r}_T^{(2)} \cdot \boldsymbol{\nabla}\right) \boldsymbol{u}^O + \left(\boldsymbol{\Delta r}_T^{(1)} \cdot \boldsymbol{\nabla}\right) \boldsymbol{u}^H + \frac{1}{2}\left(\boldsymbol{\Delta r}_T^{(1)} \cdot \boldsymbol{\nabla}\right)^2 \boldsymbol{u}^Q + \left(\boldsymbol{\Delta r}_T^{(1)} \cdot \boldsymbol{\nabla}\right)\left(\boldsymbol{\Delta r}_T^{(2)} \cdot \boldsymbol{\nabla}\right) \boldsymbol{u}^D \tag{4.16}$$

is integrated to give

$$\boldsymbol{\Delta r}_T^{(6)} = -\frac{225\pi(2Q_r(O_\perp + O_\parallel) + O_r(Q_\perp + 3Q_\parallel) + 2\kappa H_r)}{512V^2}\frac{1}{\rho^6}\hat{\boldsymbol{e}}_\phi, \tag{4.17}$$

which is purely azimuthal as for $\boldsymbol{\Delta r}_T^{(4)}$.

In summary, tracer trajectories and final displacements for large r values can be written as a series in $1/r$. We have computed contributions up to the sixth order inclusive, which gives us enough information to study a short swimming path and also the two leading order contributions along each of z, ρ and ϕ for an infinite swimming path. For a finite swimming path from $z = -L$ to $+L$, we sum the lower order contributions:

$$\boldsymbol{\Delta r}_T^{L} = -\frac{\kappa}{V}\frac{2\rho L}{r_L^3}\hat{\boldsymbol{e}}_\rho + \frac{2L^3(Q_\parallel - 2Q_\perp) - (Q_\parallel + Q_\perp)L\rho^2}{V r_L^5}\hat{\boldsymbol{e}}_z + \frac{O_r}{V}\frac{6\rho L}{r_L^5}\hat{\boldsymbol{e}}_\phi + O\left(\frac{1}{\rho^3}\right) \tag{4.18}$$

where $r_L^2 = L^2 + \rho^2$. For an infinite swimming path or close to a finite swimming path, in the limit $r_T^{int} \ll L$, we sum the higher order contributions to obtain

$$\begin{aligned}\boldsymbol{\Delta r}_T^{\infty} = &\left(-\frac{\pi\kappa^2}{16V^2}\frac{1}{\rho^3} + \frac{9\pi(9Q_\parallel^2 + 14Q_\parallel Q_\perp + 41Q_\perp^2)}{1024V^2}\frac{1}{\rho^5} - \frac{9\pi\kappa(3O_\parallel + 7O_\perp)}{256V^2}\frac{1}{\rho^5}\right)\hat{\boldsymbol{e}}_z \\ &+ \left(+\frac{9\pi\kappa Q_r}{8V^2}\frac{1}{\rho^4} - \frac{225\pi(2Q_r(O_\perp + O_\parallel) + O_r(Q_\perp + 3Q_\parallel) + 2\kappa H_r)}{512V^2}\frac{1}{\rho^6}\right)\hat{\boldsymbol{e}}_\phi \\ &+ 0\ \hat{\boldsymbol{e}}_\rho + O\left(\frac{1}{\rho^7}\right).\end{aligned} \tag{4.19}$$

These equations are analysed and discussed in §3 of in the main text.

As a final remark, we note that there is a point where analytic integration is no longer possible using this method. This happens first for the ninth order contribution. In this case the integrand contains the term $\left(\boldsymbol{\Delta r}_T^{(3)} \cdot \boldsymbol{\nabla}\right)^2 \boldsymbol{u}^D$ which is proportional to $\arctan^2(r/\rho)$. Analytically, therefore, tracer displacment can be computed exactly up to order $\boldsymbol{\Delta r}_T^{(8)}$ inclusive.

4.2. *Micro-swimmer near a no-slip boundary*

We now repeat the analysis of § 4.1 for a micro-swimmer moving along a path parallel to no-slip boundary. We include terms up to fourth order in the perturbative expansion, which are necessary to describe the leading order terms responsible for the entrainment of tracer particles close to the swimmer. Subsequently, we study the dependence of the resulting functions on the distance to the boundary H.

We begin with the leading term, given by equation MT(2.11), into which we substitute the dipolar flow field given by the first term, proportional to κ, of equation (2.16). For a swimmer moving with a constant velocity V along z, we have $(\hat{\boldsymbol{e}}_z \cdot \boldsymbol{\nabla}) = \partial_z = -V^{-1}\partial_t$. Hence, direct integration yields

$$\boldsymbol{\Delta r}_T^{(1)}(R_z) = \left[\frac{\kappa}{V}\overline{\boldsymbol{u}}_z^S\right]_{R_z^{int}}^{R_z}. \tag{4.20}$$

This result describes the first order trajectory of a tracer particle. It is a parametric function of the swimmer position R_z, or equivalenty of time $t = (R_z - R_z^{int})/V$.

Equation (4.20) can be evaluated explicitly for an arbitrary initial tracer position $(x_T^{int}, y_T^{int}, 0)$. We scale variables with respect to the the swimming height so that $x_T^{int} = \zeta H$, $y_T^{int} = \xi H$ and $R_z = \Lambda H$, giving

$$\begin{aligned}\boldsymbol{\Delta r}_T^{(1)}(\Lambda) = \frac{\kappa}{HV}\Bigg[&- \Lambda\left(\frac{\zeta-1}{\Upsilon_+^3} - \frac{\zeta-1}{\Upsilon_-^3} + \frac{6\zeta(\zeta+1)}{\Upsilon_-^5}\right)\hat{\boldsymbol{e}}_x \\ &- \xi\Lambda\left(\frac{1}{\Upsilon_+^3} - \frac{1}{\Upsilon_-^3} + \frac{6\zeta}{\Upsilon_-^5}\right)\hat{\boldsymbol{e}}_y \\ &+ \left(\frac{1}{\Upsilon_+} + \frac{\Lambda^2}{\Upsilon_+^3} - \frac{1}{\Upsilon_-} - \frac{\Lambda^2}{\Upsilon_-^3} - \frac{2\zeta}{\Upsilon_-^3} + \frac{6\Lambda^2\zeta}{\Upsilon_-^5}\right)\hat{\boldsymbol{e}}_z\Bigg]_{\Lambda^{int}}^{\Lambda}, \end{aligned} \tag{4.21}$$

where $\Upsilon_\pm^2 = {r^{(*)}}^2/H^2 = \Lambda^2 + (\zeta \mp 1)^2 + \xi^2$ in this geometry.

The second order contribution is given by integrating the quadrupolar terms of equation (2.16) in the same way as equation (4.20). Evaluated explicity this becomes

$$\boldsymbol{\Delta r}_T^{(2)}(\Lambda) = \sum_{b,c}\frac{1}{H^2V}\left[\boldsymbol{D}_{b,c}[\zeta,\xi]\ \frac{1}{\Upsilon_+^b\Upsilon_-^c}\right]_{\Lambda^{int}}^{\Lambda}, \quad \text{where } b,c \in \mathbb{N}^0, \text{ and where} \tag{4.22}$$

$$\begin{aligned}
D^x_{0,3} &= -2Q_r\xi,\\
D^x_{0,5} &= -12Q_r\zeta(1+\zeta)\xi,\\
D^x_{0,7} &= \frac{1}{2}\Big(Q_\parallel\left(3\zeta^4 - \zeta^5 + \zeta^3\left(16+\Lambda^2-2\xi^2\right) - \left(-1+2\Lambda^2-\xi^2\right)\left(1+\Lambda^2+\xi^2\right)\right.\\
&\quad \left.+\zeta^2\left(20-23\Lambda^2+4\xi^2\right) + \zeta\left(9-25\Lambda^2+2\Lambda^4+\left(8+\Lambda^2\right)\xi^2-\xi^4\right)\right)\\
&\quad +Q_\perp\left(39\zeta^4+11\zeta^5+\left(1+\Lambda^2+\xi^2\right)\left(1+4\Lambda^2+\xi^2\right)+\zeta^3\left(52+7\Lambda^2+10\xi^2\right)\right.\\
&\quad \left.+\zeta^2\left(32+43\Lambda^2+16\xi^2\right) - \zeta\left(-9-41\Lambda^2+4\Lambda^4+\left(-8+5\Lambda^2\right)\xi^2+\xi^4\right)\right)\Big),\\
D^x_{3,0} &= 2Q_r\xi,\\
D^x_{5,0} &= \frac{1}{2}(-1+\zeta)\left(Q_\parallel\left(1+(-2+\zeta)\zeta-2\Lambda^2+\xi^2\right)\right.\\
&\quad \left.+Q_\perp\left(1+(-2+\zeta)\zeta+4\Lambda^2+\xi^2\right)\right),\\
D^y_{0,5} &= 2Q_r(-1+\zeta)\left((1+\zeta)^2+\Lambda^2\right) - 2Q_r(1+5\zeta)\xi^2,\\
D^y_{0,7} &= \frac{1}{2}\xi\Big(Q_\parallel\left(2\zeta^3-\zeta^4+\zeta^2\left(6+\Lambda^2-2\xi^2\right)+2\zeta\left(1-11\Lambda^2+\xi^2\right)\right.\\
&\quad \left.+\left(-1+2\Lambda^2-\xi^2\right)\left(1+\Lambda^2+\xi^2\right)\right)\\
&\quad +Q_\perp\left(26\zeta^3+11\zeta^4-\left(1+\Lambda^2+\xi^2\right)\left(1+4\Lambda^2+\xi^2\right)+2\zeta\left(1+13\Lambda^2+\xi^2\right)\right.\\
&\quad \left.+\zeta^2\left(18+7\Lambda^2+10\xi^2\right)\right)\Big),\\
D^y_{3,0} &= -2Q_r(-1+\zeta),\\
D^y_{5,0} &= \frac{1}{2}\xi\left(Q_\parallel\left(1+(-2+\zeta)\zeta-2\Lambda^2+\xi^2\right)+Q_\perp\left(1+(-2+\zeta)\zeta+4\Lambda^2+\xi^2\right)\right),\\
D^z_{0,5} &= 12Q_r\zeta\Lambda\xi,\\
D^z_{0,7} &= \frac{1}{2}\Lambda\Big(Q_\parallel\left(-14\zeta^3+\zeta^4+2\zeta\left(-7+5\Lambda^2-7\xi^2\right)-\zeta^2\left(30+\Lambda^2-2\xi^2\right)\right.\\
&\quad \left.-\left(-1+2\Lambda^2-\xi^2\right)\left(1+\Lambda^2+\xi^2\right)\right)\\
&\quad +Q_\perp\left(-14\zeta^3-11\zeta^4+\zeta^2\left(6-7\Lambda^2-10\xi^2\right)\right.
\end{aligned}$$

$$+\left(1+\Lambda^2+\xi^2\right)\left(1+4\Lambda^2+\xi^2\right)+2\zeta\left(5-7\Lambda^2+5\xi^2\right)\big)\big),$$

$$D^z_{5,0}=\frac{1}{2}\Lambda\left(-Q_{\parallel}\left(1+(-2+\zeta)\zeta-2\Lambda^2+\xi^2\right)-Q_{\perp}\left(1+(-2+\zeta)\zeta+4\Lambda^2+\xi^2\right)\right).$$

Notice that until now the swimmer and image system flow fields have been integrated independently. They are separate solutions to the Stokes equtions, linearly superposed to fulfil the boundary conditions, and hence remain separate upon integration. Therefore the structure functions $\boldsymbol{D}_{b,c}$ have either b or c equal to zero.

At the third order contribution this is no longer the case. The equation of motion

$$\partial_t\Delta\boldsymbol{r}_T^{(3)}=\boldsymbol{u}^O+\boldsymbol{u}^{O*}+\left([\Delta\boldsymbol{r}_T^{(1)}+\Delta\boldsymbol{r}_T^{(1)*}]\cdot\boldsymbol{\nabla}\right)(\boldsymbol{u}^D+\boldsymbol{u}^{D*}) \tag{4.23}$$

contains cross-terms between the swimmer and its image system. This interference will lead to boundary effects, particularly near the surface and in the far-field, where the distance to the swimmer and the image system become comparable.

To obtain $\Delta\boldsymbol{r}_T^{(3)}$ we substitute the expressions for the dipolar flow field, given by the first term of equation (2.16), and the first order displacement, given by equation (4.21), into equation (4.23) and rewrite it as

$$\frac{d\boldsymbol{r}_T^{(3)}}{dt}=\sum_{a,b,c}\boldsymbol{C}_{a,b,c}[\zeta,\xi]\,\frac{\Lambda^a}{\Upsilon_+^b\Upsilon_-^c},\quad a,b,c\in\mathbb{N}^0 \tag{4.24}$$

where the prefactors $\boldsymbol{C}_{a,b,c}[\zeta,\xi;\ \kappa,Q,O,\ldots]$ are constant during the integration. Note that now there are coefficients with both $b,c\neq 0$ due to the cross-terms in equation (4.23). The integral of equation (4.24) with respect to the swimmer position R_z is

$$\boldsymbol{r}_T^{(3)}(R_z)=\sum_{a,b,c}\boldsymbol{C}_{a,b,c}[\zeta,\xi]\left[\frac{\Lambda^{1+a}}{1+a}\frac{1}{\rho_+^b}\frac{1}{\rho_-^c}\mathcal{A}_{F1}\left(\frac{1+a}{2},\frac{b}{2},\frac{c}{2},\frac{3+a}{2};-\frac{\Lambda^2}{\rho_+^2},-\frac{\Lambda^2}{\rho_-^2}\right)\right]_{\Lambda^{int}}^{\Lambda} \tag{4.25}$$

where $\rho_{\pm}^2=\xi^2+(\zeta\mp1)^2$ and $\mathcal{A}_{F1}$ is the first hypergeometric Appell series (see Andrews *et al.* 1999; Vidūnas 2009), provided $a-b-c<-1$ and $a\geqslant 0$. These conditions are satisfied for all terms.

Equation (4.25) may be written out explicitly for a finite swimming path, but we will not write it here in full because it is small compared to the first and second order contributions to the tracer displacement. However, in the limit of infinite swimming paths, exactly as for the swimmer in an infinite fluid, the first and second order contributions $\Delta\boldsymbol{r}_T^{(1)}$ and $\Delta\boldsymbol{r}_T^{(2)}$ vanish, and $\boldsymbol{\Delta r}_T^{(3)}$ becomes the leading order contribution to the tracer displacement. In this limit of $R_z^{int}=-\infty$ to $R_z=\infty$ the hypergeometric Appell series reduce to simpler functions such as polynomials or the complete elliptic integrals $\mathcal{E}[m]$ and $\mathcal{K}[m]$ (defined in Arfken & Weber 2005, p. 332). The resulting expression is

$$\boldsymbol{r}_T^{(3)}=\frac{\kappa^2}{H^3V^2}\left[h_0(\xi,\zeta)+h_1(\xi,\zeta)\mathcal{K}\left(\frac{4\zeta}{\rho_-^2}\right)+h_2(\xi,\zeta)\mathcal{E}\left(\frac{4\zeta}{\rho_-^2}\right)\right]\hat{\boldsymbol{e}}_z, \tag{4.26}$$

where the structure functions $h_{0,1,2}(\xi,\zeta)$ are

$$h_0=-\frac{\pi}{1024}\left(\frac{64}{\rho_+^3}-\frac{515}{\rho_-^3}+\frac{96+1254r_-^2}{\rho_-^5}-\frac{675}{\rho_-^7}\right), \tag{4.27}$$

$$h_1=\frac{1}{\rho_-}\frac{\zeta^3-3\zeta^4+2\zeta\left(1+\xi^2\right)-18\left(1+\xi^2\right)^2-\zeta^2\left(10+21\xi^2\right)}{4\zeta^4}, \tag{4.28}$$

$$h_2=\frac{1}{\rho_+^2\rho_-}\Bigg(\frac{-\zeta^5+3\zeta^6-3\zeta^3\left(-1+\xi^2\right)-2\zeta\left(1+\xi^2\right)^2+18\left(1+\xi^2\right)^3}{4\zeta^4}$$

$$+\frac{\zeta^4\left(5+24\xi^2\right)+13\zeta^2\left(-2+\xi^2+3\xi^4\right)}{4\zeta^4}\Bigg). \tag{4.29}$$

To investigate the behaviour of equation (4.26) close to the boundary we expand the elliptic integrals for small ζ values.

$$\mathcal{K}\left[\frac{4\zeta}{r_+^2}\right]=\frac{\pi}{2}+\frac{\pi}{2(1+\xi^2)}\zeta+\frac{17\pi}{8(1+\xi^2)^2}\zeta^2+\mathcal{O}\left(\zeta^3\right) \tag{4.30}$$

$$\mathcal{E}\left[\frac{4\zeta}{r_+^2}\right]=\frac{\pi}{2}-\frac{\pi}{2(1+\xi^2)}\zeta-\frac{11\pi}{8(1+\xi^2)^2}\zeta^2+\mathcal{O}\left(\zeta^3\right). \tag{4.31}$$

On the other hand, expanding the elliptic integrals for large ζ values yields

$$\mathcal{K}\left[\frac{4\zeta}{r_+^2}\right]=\frac{\pi}{2}+\frac{\pi}{2}\frac{1}{\zeta}+\frac{17\pi}{8}\frac{1}{\zeta^2}+\mathcal{O}\left(\frac{1}{\zeta^3}\right) \tag{4.32}$$

$$\mathcal{E}\left[\frac{4\zeta}{r_+^2}\right]=\frac{\pi}{2}-\frac{\pi}{2}\frac{1}{\zeta}-\frac{11\pi}{8}\frac{1}{\zeta^2}+\mathcal{O}\left(\frac{1}{\zeta^3}\right) \tag{4.33}$$

which may be used to study the behaviour of equation (4.26) in the far-field.

The fourth order contribution follows from equation MT(2.14). The first term on the RHS is a perfect differential and last two terms can be integrated using the same method as for $\boldsymbol{\Delta r}_T^{(3)}$. For an infinite swimming path the result is a contribution perpendicular to the swimming direction:

$$\boldsymbol{\Delta r}_T^{(4)}=\frac{\kappa Q_r}{H^4V^2}\left[h_{11}(\xi,\zeta)\hat{\boldsymbol{e}}_x+h_{12}(\xi,\zeta)\hat{\boldsymbol{e}}_y\right]+\frac{\kappa Q_\perp}{H^4V^2}\left[h_{21}(\xi,\zeta)\hat{\boldsymbol{e}}_x+h_{22}(\xi,\zeta)\hat{\boldsymbol{e}}_y\right], \tag{4.34}$$

where the full expressions for the functions h_{ij} are available from the authors. Nonetheless, all contributions up to fourth order are discussed in SI-§6.

4.3. *Micro-swimmer near a free-slip boundary*

Now we repeat the calculations of §4.2 for the case of a micro-swimmer moving along a line parallel to a free-slip boundary. Using the flow field, given by equation (2.14), we compute the first and second order contributions in terms of the scaled coordinates.

$$\boldsymbol{\Delta r}_T^{(1)}(\Lambda)=\frac{\kappa}{HV}\left[\frac{\left\{(1-\zeta)\Lambda,-\xi\Lambda,\Upsilon_+^2+\Lambda^2\right\}}{\Upsilon_+^3}+\frac{\left\{-(\zeta+1)\Lambda,-\xi\Lambda,\Upsilon_-^2+\Lambda^2\right\}}{\Upsilon_-^3}\right]_{\Lambda^{int}}^{\Lambda} \tag{4.35}$$

and similarly

$$\begin{aligned}\boldsymbol{\Delta r}_T^{(2)}(\Lambda)=&\frac{Q_\parallel}{H^2V}\left[\left(\frac{\Upsilon_+^2-3\Lambda^2}{2\Upsilon_+^5}\right)\{\zeta-1,\xi,-\Lambda\}+\left(\frac{\Upsilon_-^2-3\Lambda^2}{2\Upsilon_-^5}\right)\{\zeta+1,\xi,-\Lambda\}\right]_{\Lambda^{int}}^{\Lambda}\\&+\frac{Q_\perp}{H^2V}\left[\left(\frac{\Upsilon_+^2+3\Lambda^2}{2\Upsilon_+^5}\right)\{\zeta-1,\xi,-\Lambda\}+\left(\frac{\Upsilon_-^2+3\Lambda^2}{2\Upsilon_-^5}\right)\{\zeta+1,\xi,-\Lambda\}\right]_{\Lambda^{int}}^{\Lambda}\\&+\frac{Q_r}{H^2V}\left[-\frac{2\{-\xi,\zeta-1,0\}}{\Upsilon_+^3}+\frac{2\{-\xi,\zeta+1,0\}}{\Upsilon_-^3}\right]_{\Lambda^{int}}^{\Lambda}.\end{aligned} \tag{4.36}$$

In the limit of infinite swimming paths the first and second order contributions vanish and, as before, the third order contribution becomes the leading term. Hence, integrating equation (4.23) for a free-slip boundary gives

$$\boldsymbol{\Delta r}_T^{(3)}=\frac{\kappa^2}{16H^3V^2}\left[g_0(\xi,\zeta)+g_1(\xi,\zeta)\mathcal{K}\left(\frac{4\zeta}{\rho_-^2}\right)+g_2(\xi,\zeta)\mathcal{E}\left(\frac{4\zeta}{\rho_-^2}\right)\right]\hat{\boldsymbol{e}}_z, \tag{4.37}$$

where the structure functions $g_{0,1,2}(\xi,\zeta)$ are

$$g_0 = -\pi\left(\rho_+^3+\rho_-^3\right)/\rho_+^3\rho_-^3, \tag{4.38}$$

$$g_1 = +4\rho_-^{-1}\left(1-(3+5\xi^2)\zeta^{-2}-6(1+\xi^2)^2\zeta^{-4}\right), \tag{4.39}$$

$$g_2 = -4\rho_+^{-2}\rho_-^{-1}\left(\zeta^2-4(1+\xi^2)+(9-2\xi^2-11\xi^4)\zeta^{-2}-6(1+\xi^2)^3\zeta^{-4}\right). \tag{4.40}$$

The fourth order contribution to the final tracer displacement for an infinite swimming path is perpendicular to the swimming direction.

$$\boldsymbol{\Delta r}_T^{(4)} = \frac{\kappa Q_r}{H^4V^2}\left[g_{11}(\xi,\zeta)\hat{\boldsymbol{e}}_x+g_{12}(\xi,\zeta)\hat{\boldsymbol{e}}_y\right]+\frac{\kappa Q_\perp}{H^4V^2}\left[g_{21}(\xi,\zeta)\hat{\boldsymbol{e}}_x+g_{22}(\xi,\zeta)\hat{\boldsymbol{e}}_y\right], \tag{4.41}$$

where the structure functions g_{ij} are given by Mathijssen (2016) and discussed in SI-§ 5.

5. Analytical results: swimmer moving parallel to a free-slip boundary

In § 4.3 we calculated the tracer displacement in equation (4.2) up to the fourth order contribution, $\boldsymbol{\Delta r}_T^{(1-4)}$. Analogous to equation MT(3.1) we consider a swimming path of finite length between $z=-L$ and $+L$ a distance $x=H$ from the boundary, and we consider tracers initially located in the $z=0$ plane. Adding up the lowest order contributions to the tracer displacement, given by equations (4.35)-(4.36), yields

$$\begin{aligned}\boldsymbol{\Delta r}_T^{L,H} = &-\frac{2\kappa\Lambda}{HV}\left(\frac{(\zeta-1)\hat{\boldsymbol{e}}_x+\xi\hat{\boldsymbol{e}}_y}{\Upsilon_+^3}+\frac{(\zeta+1)\hat{\boldsymbol{e}}_x+\xi\hat{\boldsymbol{e}}_y}{\Upsilon_-^3}\right)\\ &+\frac{Q_\parallel\Lambda}{H^2V}\left(\frac{3\Lambda^2-\Upsilon_+^2}{\Upsilon_+^5}+\frac{3\Lambda^2-\Upsilon_-^2}{\Upsilon_-^5}\right)\hat{\boldsymbol{e}}_z\\ &-\frac{Q_\perp\Lambda}{H^2V}\left(\frac{3\Lambda^2+\Upsilon_+^2}{\Upsilon_+^5}+\frac{3\Lambda^2+\Upsilon_-^2}{\Upsilon_-^5}\right)\hat{\boldsymbol{e}}_z\\ &+0\frac{Q_r}{H^2V}+\mathcal{O}\left(\frac{1}{H^3}\right),\end{aligned} \tag{5.1}$$

where $\zeta=x_T^{int}/H$, $\xi=y_T^{int}/H$, $\Lambda=L/H$ and $\Upsilon_\pm^2=\Lambda^2+(\zeta\mp1)^2+\xi^2$. The leading order dipole term, as in the case for an unbounded swimmer, attracts the tracers towards the swimming path and towards the image swimming path in the radial direction. Between the swimmer and the boundary these terms compete, but elsewhere there is cooperation and the tracer trajectories are doubled in size. The quadrupolar terms give the leading order contribution in the longitudinal direction, and the swimmer and image cooperate. Finally, the rotlet doublet terms cancel by symmetry.

When the swimming path length $2L$ tends to infinity, the tracer trajectories form almost closed loops and the final tracer displacement tends to a constant value. The first and second order contributions to the final displacement both decay as $\boldsymbol{\Delta r}_T^{(1,2)}\propto L^{-2}$ in the limit $L\gg|\boldsymbol{r}_T^{int}-H\hat{\boldsymbol{e}}_x|$, *i.e.* the limit of particles located close to the centre of the swimming path with respect to L. The third order contribution remains finite in this limit, however, and hence becomes the leading order.

In the case of swimming near a boundary this limit $L\gg|\boldsymbol{r}_T^{int}-H\hat{\boldsymbol{e}}_x|$ is still a good assumption close to the boundary but, if the swimming path is finite, not in the far-field where the lower order contributions $\boldsymbol{\Delta r}_T^{(1-2)}$ given by equation (5.1) are dominant.

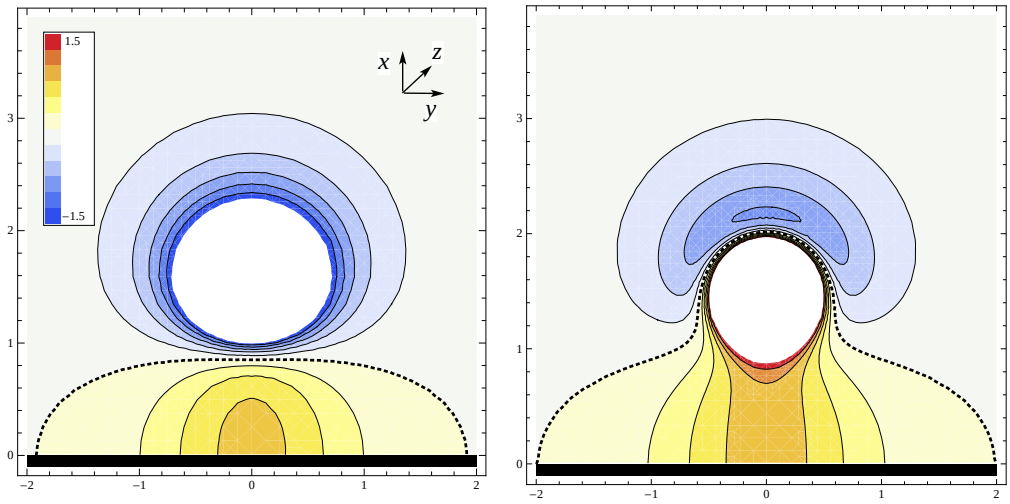

(a) Purely dipolar swimmer

(b) Dipole and quadrupole

Figure 5: Analytical results for longitudinal tracer displacement near a free-slip boundary for an infinite swimming path, as seen in the (x, y) plane where $\hat{\boldsymbol{e}}_z$ points into the paper. The units of length and time are μm and s. Parameters used are $\kappa = 30, V = 20, H = 1.5$. Colours indicate the magnitude of the displacement in the swimming direction. White indicates the region close to the swimmer where the value $|\boldsymbol{\Delta r}_T^z| > 1.5$. The thick black line indicates the boundary. Contours have spacing 0.25 and the dotted black line is the zero-contour. (a) The leading order contribution $\boldsymbol{\Delta r}_T^{(3)}$, given by equation (4.37). (b) Adding the quadrupolar terms of $\boldsymbol{\Delta r}_T^{(5)}$ allows to include the effects of the positive near-field entrainment. We have chosen $Q_{\parallel,\perp} = 6$, corresponding to an entrainment radius, given by equation MT(3.4), of $\rho_c = 0.6\mu$m.

5.1. *Longitudinal component of the tracer displacement*

Consider the final displacement in the swimming direction, $\hat{\boldsymbol{e}}_z$. The leading order contribution for an infinite swimming path length in this direction is plotted in figure 5a. This solution $\boldsymbol{\Delta r}_T^{(3)}$ is given by equation (4.37), in terms of $\zeta = x_T^{int}/H$ and $\xi = y_T^{int}/H$. The fourth order contribution cancels in this directions, so corrections are $O\left(\boldsymbol{\Delta r}_T^{(5)}\right)$.

Firstly, the result for a swimmer in the bulk, given by equation (4.19), is recovered close to the swimming path, as expected. If the expression for $\boldsymbol{\Delta r}_T^{(3)}$ given by (4.37) is expanded about the point $x = H$ then we obtain equation (4.11), and similarly for higher order terms. Secondly, the image is simply another swimmer rotating in the opposite direction. Thirdly, however, the tracer displacement is not just the sum of the swimmer and image solutions. That is due to the cross-terms in equation (4.23) between the swimmer and the image. This is apparent at the boundary itself. Here the displacement is not negative as would be predicted simply by adding the swimmer and image dipolar contributions, given by equation (4.11). Instead, there is positive forward-displacement at the boundary.

A leading order expression can be obtained for the tracer displacement at the boundary by taking the limit $\zeta \to 0$ in equation (4.37) (see e.g. Arfken & Weber 2005, p. 333 for a series expansion of the elliptic integrals), giving

$$\lim_{\zeta \to 0} \boldsymbol{\Delta r}_T^{(3)} = \frac{\kappa^2}{V^2 H^3} \frac{\pi\left(13 - 8\xi^2\right)}{32\left(1 + \xi^2\right)^{5/2}} \hat{\boldsymbol{e}}_z. \tag{5.2}$$

This function has a maximum at the origin with value

$$\lim_{\zeta\to 0}\ \lim_{\xi\to 0} \boldsymbol{\Delta r}_T^{(3)} = \frac{13\pi\kappa^2}{32V^2H^3}\ \hat{\boldsymbol{e}}_z, \tag{5.3}$$

which evaluates to 0.85μm for the parameters used in figure 5a.

Other properties can also be derived analytically. The zero-contour intersects the boundary at $\xi_0 = \pm\sqrt{13/8} \approx \pm 1.27$. Similarly, it intersects the x-axis at $\zeta_0 = 0.568$, independent of the swimmer coefficients κ and V. At the boundary the displacement reaches minima at $\xi_{min} = \pm\sqrt{27/8} \approx \pm 1.84$ and eventually decays to zero according to

$$\lim_{\zeta\to 0}\ \lim_{\xi\to +\infty} \boldsymbol{\Delta r}_T^{(3),z} = -\frac{\pi\kappa^2}{4V^2H^3}\frac{1}{|\xi|^3}. \tag{5.4}$$

Far away from the boundary and swimming path the longitudinal displacement is negative. In the limit of large ρ values, where $\rho^2 = \xi^2 + \zeta^2$, we find the same far-field scaling as given by equation (5.4) with $|\xi| \to \rho$. This is exactly four times the free swimmer result, given by equation (4.19). These are equal contributions from the swimmer and its image, and from each of the cross-terms in equation (4.23).

Hence, the free-slip boundary affects the longitudinal displacement significantly. Close to the boundary tracers are moved forwards with the swimmer, contrary to the free swimmer result. In the far-field tracers are moved backwards, as for the free swimmer, but with displacements enhanced by a factor of four.

Near-field entrainment effects may be estimated by adding the quadrupolar terms from the fifth order contribution $\boldsymbol{\Delta r}_T^{(5)}$, as shown in figure 5b. At the boundary and in the far-field the dipolar results hold. Closer to the swimming path the numerical results shown in figure MT7b are reproduced. The near-field entrainement and the forward-displacement at the boundary interfere when the entrainment radius ρ_c, given by equation MT(3.4), is comparable in magnitude to H. In that case, because the quadrupolar terms are always positive, the forward-displacement at the boundary is enhanced further, as shown in figure 7c of the main text.

5.2. *Transverse components of the tracer displacement*

Now we consider the transverse components of the tracer displacement, along x and y. For an infinite swimming path the leading order term is the fourth order contribution $\boldsymbol{\Delta r}_T^{(4)}$, given by equation (4.41). This expression contains two terms. The first, proportional to κQ_r, is due to the rotation of the swimmer's head and tail, as we have described for a swimmer in the bulk in § 3.2 of the main text. The second term of equation (4.41) however, proportional to $\kappa Q_\perp$, is due to the interaction between the swimmer and its image, and exists also for non-rotating swimmers.

Figure 6a shows the azimuthal displacement for a rotating swimmer. It rotates fluid particles about the swimmer axis, like a swimmer in an infinite fluid given by equation (4.19), but the displacement is enhanced at the boundary by the image. Figure 6b shows a non-rotating swimmer, generating a completely new type of displacement that did not exist for swimmers in an unbounded fluid. This displacement has the structure of an electric dipole field, centered at the swimming path and aligned in the $-x$ direction. These transverse displacements could be a mechanism for re-suspending sedimented particles back into the bulk fluid.

Therefore, to study the tracer displacement at the boundary quantitatively, we take

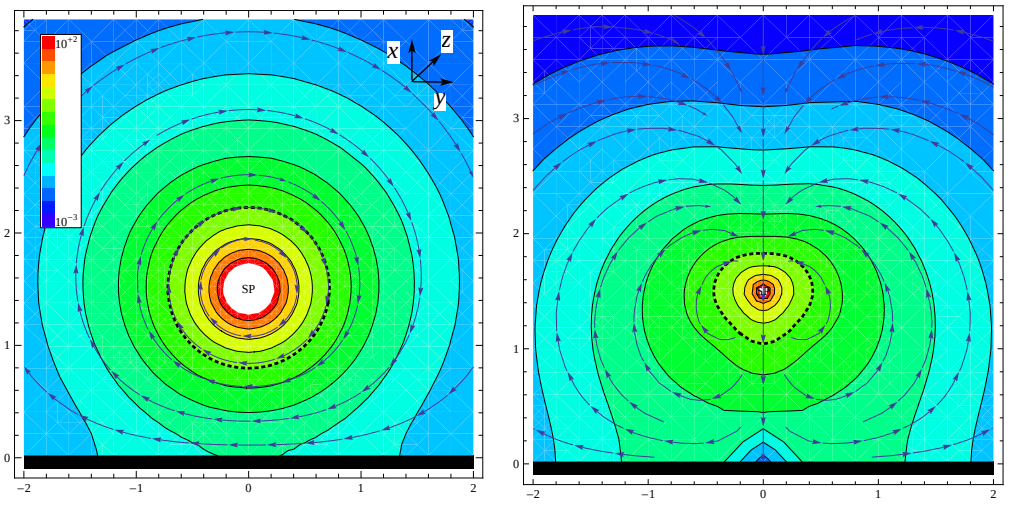

(a) $Q_r = 1, Q_{\parallel,\perp} = 0$ (b) $Q_r = 0, Q_{\parallel,\perp} = 10$

Figure 6: Analytical results for the tracer displacement $\boldsymbol{\Delta r}_T^{(4)}$ along the transverse directions for an infinite swimming path along a free-slip boundary, as seen in the (x, y) plane. $\hat{\boldsymbol{e}}_z$ points into the paper. The units of length and time are μm and s. Parameters used are $\kappa = 30, V = 20, H = 1.5$. Arrows indicate the direction of the transverse tracer displacement. Colours portray the base-10 logarithm of the norm of this transverse displacement ranging from -3 (violet) to $+2$ (red). The dotted black line is the contour of 1μm displacement. White indicates the singularity centre close to the swimmer. The thick black line indicates the boundary. (a) A swimmer with oppositely rotating head and tail. (b) A non-rotating swimmer.

the limit $\zeta \to 0$ in equation (4.41), giving

$$\lim_{\zeta \ll 1} \boldsymbol{\Delta r}_T^{(4)} = -\frac{3\pi\kappa}{16H^4V^2} \frac{7Q_r - 5Q_\perp \xi + 17Q_r\xi^2}{(\xi^2+1)^{7/2}}\, \hat{\boldsymbol{e}}_y - \frac{15\pi\kappa}{16H^4V^2} \frac{Q_\perp - 6Q_\perp\xi^2 + Q_r\xi\left(3+17\xi^2\right)}{(\xi^2+1)^{9/2}} \zeta\, \hat{\boldsymbol{e}}_x + O\left(\zeta^2\right) \tag{5.5}$$

For a rotating swimmer (with $Q_\perp = 0$) the component along y is even in ξ with an extremum at the origin, with magnitude

$$\lim_{\zeta \to 0} \lim_{\xi \to 0} \boldsymbol{\Delta r}_T^{(4)} = -\frac{21\pi\kappa Q_r}{16H^4V^2} \hat{\boldsymbol{e}}_y. \tag{5.6}$$

Therefore, the azimuthal tracer displacement is increased by a factor of 7/6 at the free-slip boundary compared to the result for a swimmer in the bulk, given by equation (4.13). The x-component is maximised at $\xi_n = \pm\frac{1}{2}\sqrt{\frac{1}{17}\left(9+\sqrt{217}\right)} = \pm 0.591$ where the value is

$$\lim_{\zeta \ll 1} \lim_{\xi \to \xi_n} \boldsymbol{\Delta r}_T^{(4)} = \mp 1.37 \frac{15\pi\kappa Q_r}{16H^4V^2} \zeta \hat{\boldsymbol{e}}_x. \tag{5.7}$$

For a non-rotating swimmer (with $Q_r = 0$) there is a stagnation point at $\xi = 0$. The displacement along y is maximised at $\xi = \pm 1/\sqrt{6} \approx \pm 0.41$ where the value is $\pm\frac{405\pi\kappa Q_\perp}{686\sqrt{7}V^2H^4}\hat{\boldsymbol{e}}_y$ and the displacement along x is maximised at $\xi = \pm 1/\sqrt{2} \approx \pm 0.71$ where

the value is $+0.323\frac{15\pi\kappa Q_\perp \zeta}{16H^4V^2}\hat{\boldsymbol{e}}_x$. Using this analysis, we can identify the maxima in the tracer displacement as the regions where the tracer mixing is optimised. Far away from the swimmer but on the boundary, in the limit $\xi \to \infty$, equation (5.5) tends to

$$\lim_{\zeta\to 0}\lim_{\xi\to+\infty}\boldsymbol{\Delta r}_T^{(4),y} = -\frac{51\pi\kappa Q_r}{16V^2H^4}\frac{1}{\xi^5} + \frac{15\pi\kappa Q_\perp}{16V^2H^4}\frac{1}{\xi^6} + O(\xi^{-7}). \tag{5.8}$$

Far away from both boundary and swimming path, where $\zeta \to \infty$, the displacement in the x and y directions tends to

$$\lim_{\zeta\to+\infty}\lim_{\xi\to 0}\boldsymbol{\Delta r}_T^{(4)} = +\frac{51\pi\kappa Q_r}{4V^2H^4}\frac{1}{\zeta^5} + O(\zeta^{-7})\hat{\boldsymbol{e}}_y - \frac{15\pi\kappa Q_\perp}{16V^2H^4}\frac{1}{\zeta^6} + O(\zeta^{-8})\hat{\boldsymbol{e}}_x, \tag{5.9}$$

Hence, it is clear that far from the swimmer, for large ζ values, the Q_r term dominates with a scaling of $1/\zeta^5$. For the free swimmer the far-field scaling was $1/\zeta^4$, given by equation (4.19). It is sensible that the scaling in the transverse directions decays more quickly with the boundary present, due to the cancelling swimmer and image flow fields.

In conclusion, a free-slip boundary has a complicated effect on the transverse tracer displacement. The rotation of tracers about the swimming axis found for a swimmer in the bulk, proportional to Q_r, is increased at the boundary but decreased far from the swimmer. Additionally, tracers experience another displacement proportional to $Q_\perp$ that takes the shape of the electric dipole field, and therefore a non-rotating swimmer can still mix particles in the transverse directions. Together, these terms lead to a complex structure of stagnation points and maxima in displacement at the boundary that can be analysed using equation (5.5). This allows to make quantitative estimates in what regions the mixing is the strongest, and how much tracer particles that have stuck to or sedimented onto the surface could be mixed back into the bulk fluid.

6. Analytical results: swimmer moving parallel to a no-slip boundary

In § 5 we presented analytical results for the tracer displacement due a micro-swimmer moving parallel to a free-slip boundary. Here we repeat this analysis for a no-slip boundary. In § 4.2 we calculated the tracer displacement in equation (4.2) up to the fourth order contribution, $\boldsymbol{\Delta r}_T^{(1-4)}$. Exactly as in equations MT(3.1) and (6.1) we consider a swimming path of finite length between $z = -L$ and $+L$ a distance $x = H$ from the boundary, and we consider tracers initially located in the $z = 0$ plane. In this geometry the lowest order terms for the tracer displacement, given by equations (4.21)-(4.22), simplify substantially since only the coefficients $D^z_{0,5}$, $D^z_{0,7}$ and $D^z_{5,0}$ do not vanish:

$$\begin{aligned}
\boldsymbol{\Delta r}_T^{L,H} = &-\frac{2\kappa\Lambda}{HV}\left[\left(\frac{\zeta-1}{\Upsilon_+^3} - \frac{\zeta-1}{\Upsilon_-^3} + \frac{6\zeta(\zeta+1)}{\Upsilon_-^5}\right)\hat{\boldsymbol{e}}_x + \xi\left(\frac{1}{\Upsilon_+^3} - \frac{1}{\Upsilon_-^3} + \frac{6\zeta}{\Upsilon_-^5}\right)\hat{\boldsymbol{e}}_y\right] \\
&+ \frac{Q_\parallel\Lambda}{H^2V}\Bigg(-\frac{\zeta^2-2\zeta-2\Lambda^2+\xi^2+1}{\Upsilon_-^5} + \frac{\zeta^4-14\zeta^3-\zeta^2\left(\Lambda^2-2\xi^2+30\right)}{\Upsilon_+^7} \\
&\qquad + \frac{2\zeta\left(5\Lambda^2-7\left(\xi^2+1\right)\right)-2\Lambda^4-\Lambda^2\left(\xi^2+1\right)+\left(\xi^2+1\right)^2}{\Upsilon_+^7}\Bigg)\hat{\boldsymbol{e}}_z \\
&+ \frac{Q_\perp\Lambda}{H^2V}\Bigg(-\frac{\zeta^2-2\zeta+4\Lambda^2+\xi^2+1}{\Upsilon_-^5} + \frac{-11\zeta^4-14\zeta^3+\zeta^2\left(-7\Lambda^2-10\xi^2+6\right)}{\Upsilon_+^7} \\
&\qquad + \frac{-2\zeta\left(7\Lambda^2-5\left(\xi^2+1\right)\right)+4\Lambda^4+5\Lambda^2\left(\xi^2+1\right)+\left(\xi^2+1\right)^2}{\Upsilon_+^7}\Bigg)\hat{\boldsymbol{e}}_z
\end{aligned}$$

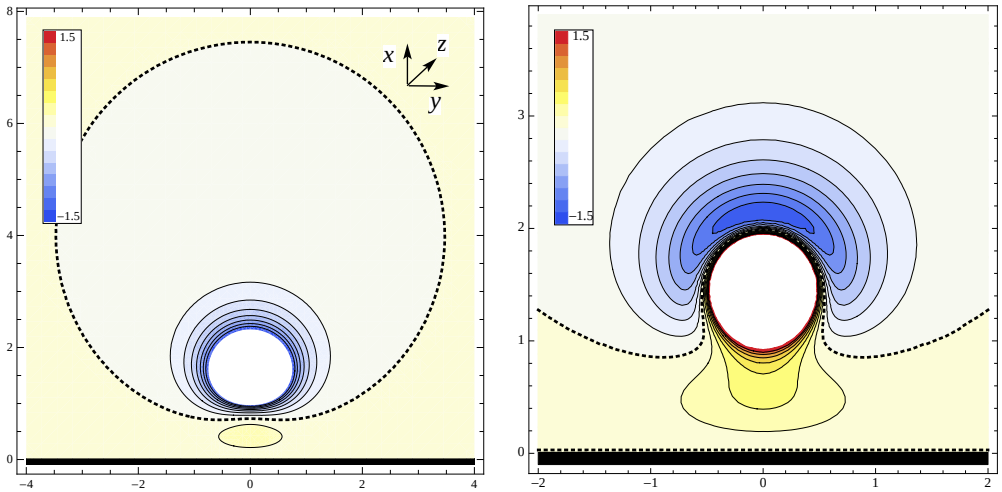

(a) Purely dipolar swimmer (b) Dipole and quadrupole

Figure 7: Analytical results for longitudinal tracer displacement near a no-slip boundary for an infinite swimming path. This figure is completely analogous to figure 5 for the free-slip boundary. Exactly the same parameters have been used for direct comparison.

$$+\frac{24Q_r\Lambda}{H^2V}\frac{\zeta\xi}{\Upsilon_+^5}\hat{\boldsymbol{e}}_z+\mathcal{O}\left(\frac{1}{H^3}\right). \tag{6.1}$$

The dipole terms of order $\Upsilon_\pm^{-3}$ attract tracers towards the swimming path but repel them from the image swimming path in the radial direction. Between the swimmer and the boundary these terms cooperate, but in the far-field they cancel in such a way that the higher order $\Upsilon_\pm^{-5}$ term attracts the tracers weakly towards the origin. The quadrupolar terms, including the rotlet doublet term, give the leading order contribution in the longitudinal direction.

As for the free-slip boundary the first and second order contributions both decay as $\boldsymbol{\Delta r}_T^{(1,2)} \propto L^{-2}$ in the limit $L \gg |\boldsymbol{r}_T^{int} - H\hat{\boldsymbol{e}}_x|$. The third order contribution given by equation (4.26) remains finite in this limit, however, and hence becomes the leading order. This limit $L \gg |\boldsymbol{r}_T^{int} - H\hat{\boldsymbol{e}}_x|$ is also justified for tracers located close to the centre of a finite swimming path and close to a boundary, but not in the far-field where the lower order contributions $\boldsymbol{\Delta r}_T^{(1-2)}$ given by equation (6.1) are dominant if L is finite.

6.1. *Longitudinal component of the tracer displacement*

We start by considering the final tracer displacement in the swimming direction, $\hat{\boldsymbol{e}}_z$. The leading order term is the third order contribution $\boldsymbol{\Delta r}_T^{(3)}$ given by equation (4.26). Notice that this expression has a prefactor proportional to κ^2/V^2H^3 multiplied by a structure function in terms of the scaled variables $\zeta = x_T^{int}/H$ and $\xi = y_T^{int}/H$. Its value is shown pictorally in figure 7a.

As for the free-slip boundary shown in figure 5a, the result for a swimmer in an unbounded fluid, given by equation (4.19), is recovered close to the swimming path. The image terms are, however, more complex in this case, as well as the cross-terms between the swimmer and the image in equation (4.23). At the boundary itself this ensures the no-slip condition. At small distances from the boundary tracers are displaced forwards in the swimming direction, as for the free-slip boundary, opposing the dipolar contribution close to the swimmer, given by equation (4.11).

To study the tracer displacement close to the boundary for an infinitely long swimming path, we expand equation (4.26) in small ζ values

$$\lim_{\zeta\ll 1} \boldsymbol{\Delta r}_T^{(3)} = \frac{\kappa^2}{V^2H^3}\frac{45\pi\left(31+24\xi^2\right)}{128\left(1+\xi^2\right)^{9/2}}\zeta^2 + O(\zeta^3) \quad \hat{\boldsymbol{e}}_z. \tag{6.2}$$

Hence, the displacement near the no-slip boundary increases quadratically with ζ.

Next, we take the limit $\xi \to 0$ in equation (4.26). The resulting function of ζ written in terms of the elliptic integrals can be studied numerically, where the numbers can be computed to arbitrary precision. The longitudinal displacement is maximised at $\zeta_m = 0.288$ where it reaches the value

$$\lim_{\zeta\to\zeta_m} \boldsymbol{\Delta r}_T^{(3)} = \frac{0.429\kappa^2}{V^2H^3}\ \hat{\boldsymbol{e}}_z, \tag{6.3}$$

which is a factor 3 less than for free-slip boundary, given by equation (5.3). For the parameters used in figure 7a, $\boldsymbol{\Delta r}_T^{(3)}$ evaluates to 0.29μm at the point $x_T^{int} = 0.43\mu$m.

The displacement changes sign at $\zeta_a = 0.487$, from positive by the maximum to negative near the swimming path. On the other side of the swimming path, at $\zeta_b = 4.97$, the displacement changes sign again from negative to positive in the far-field. The zero-contour, displayed as the thick dashed line in figure 7a, can be approximated by a circle centered at $(\zeta_a+\zeta_b)H/2$ with radius $(\zeta_b-\zeta_a)H/2$.

We consider the far-field by expanding equation (4.26) for large ζ values

$$\lim_{\zeta\gg 1} \boldsymbol{\Delta r}_T^{(3)} = +\frac{135\pi\kappa^2}{16V^2H^3}\frac{1}{\zeta^5} + O(\zeta^{-6}) \quad \hat{\boldsymbol{e}}_z. \tag{6.4}$$

Compared to a swimmer in an unbounded fluid or near a free-slip boundary, see equations (4.19) and (5.4) respectively, the far-field displacement decays faster for the no-slip boundary. This is understood as the dipolar terms of the flow field of the swimmer and its image, both scaling as $1/\zeta^3$, cancel so that the higher order terms of the flow field of the image, scaling as $1/\zeta^5$, remain.

In summary, the presence of a no-slip boundary induces forward-entrainment of tracer particles between the swimming path and the boundary. Compared to the free-slip boundary this is less by a factor of $13\pi/(32\times 0.429) \approx 3$ because of the no-slip condition, but it is still significant. Also far away from the swimming path the tracers are displaced forwards along the swimming direction.

Finally, we note that near-field entrainment effects may be estimated by adding the quadrupolar terms from the fifth order contribution $\boldsymbol{\Delta r}_T^{(5)}$, as shown in figure 7b. As in section 6, at the boundary and in the far-field the dipolar results hold. Closer to the swimming path, however, this higher order contributions becomes significant and hence the numerical results shown in figure 6b of the main text are reproduced. Because the quadrupolar terms are always positive, the dipolar forward-displacement near the boundary is enhanced further.

6.2. *Transverse components of the tracer displacement*

We now consider the components of the final tracer displacement along x and y. The third order terms $\boldsymbol{\Delta r}_T^{(3)}$ do not contribute in this direction. Hence, the leading order terms of the angular dependence are of fourth order, $\boldsymbol{\Delta r}_T^{(4)}$, given by equation (4.34) with different structure functions g_{ij} compared to the free-slip boundary. The two terms, proportional to κQ_r and $\kappa Q_\perp$ respectively, are displayed in figure 8.

Figure 8a shows that a rotating swimmer, that generates a dipolar and rotlet quadrupo-

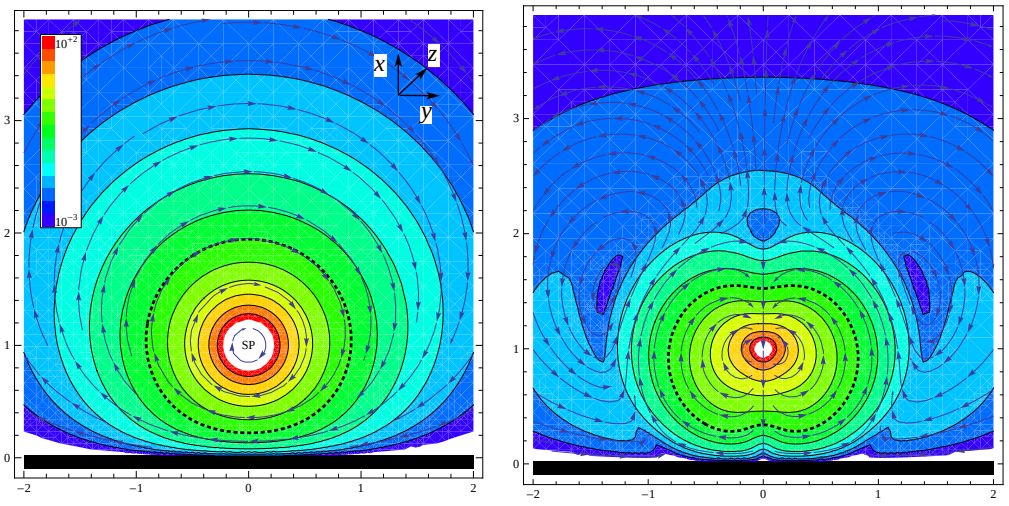

(a) $Q_r = 1, Q_{\parallel,\perp} = 0$ (b) $Q_r = 0, Q_{\parallel,\perp} = 10$

Figure 8: Analytical results for the leading order tracer displacement $\boldsymbol{\Delta r}_T^{(4)}$ along the transverse directions for an infinite swimming path along a no-slip boundary, as seen in the (x, y) plane. $\hat{\boldsymbol{e}}_z$ points into the paper. The units of length and time are μm and s. Parameters used are $\kappa = 30, V = 20, H = 1$. Arrows indicate the direction of the transverse tracer displacement. Colours portray the base-10 logarithm of the norm of this transverse displacement ranging from -3 (violet) to $+2$ (red). The dotted black line is the contour of 1μm displacement. White indicates the singularity centre close to the swimmer. The thick black line indicates the boundary. (a) A swimmer with oppositely rotating head and tail. (b) A non-rotating swimmer.

lar flow field, rotates fluid particles about the swimming path, as seen for the swimmer in the bulk or near a free-slip boundary. However, the no-slip boundary inhibits the displacement near the boundary. The image rotates tracers in the same clock-wise direction, and hence the terms cancel at $\zeta = 0$.

Figure 8b shows that for a non-rotating swimmer, with a dipolar and a perpendicular-quadrupolar flow field, the displacement close to the swimming path is the same as for the free-slip boundary. In the far-field, on the other hand, the displacement is reversed in direction. Notice that the positions in the ξ, ζ plane are scaled w.r.t. H.

The leading order expression for the transverse displacement close to the boundary is obtained by Taylor expanding equation (4.41) for small values of ζ.

$$\begin{aligned}\lim_{\zeta \ll 1} \boldsymbol{\Delta r}_T^{(4)} = &- \frac{945\pi\kappa Q_r}{128 H^4 V^2} \frac{\left(7 - 2\gamma\xi + 19\xi^2 + 4\gamma\xi^3\right)}{\left(\xi^2+1\right)^{11/2}} \zeta^2 + O(\zeta^3)\ \hat{\boldsymbol{e}}_y \\ &- \frac{315\pi\kappa Q_r}{128 H^4 V^2} \frac{3\xi\left(13 + 57\xi^2\right) + \gamma\left(2 - 32\xi^2 + 32\xi^4\right)}{\left(\xi^2+1\right)^{13/2}} \zeta^3 + O(\zeta^4)\ \hat{\boldsymbol{e}}_x, \quad (6.5)\end{aligned}$$

where $\gamma = Q_\perp / Q_r$. This expression also grows quadratically with ζ in the y direction, as for the longitudinal displacement given by equation (6.2). In the x direction the leading order term scales as ζ^3. We compare this to the case of the free-slip boundary, given by equation (5.5), where the transverse displacement scales as ζ^0 and ζ in the y and x directions respectively.

Using equation (6.5), like we described for the free-slip boundary, we can estimate the

amount of particles sedimented onto the no-slip boundary that can be re-suspended into the bulk fluid. Importantly, this now depends strongly on the particle radius, a_p. Since the centre of a sedimented particle is initially located at $\zeta = a_p$, with $a_p \ll H$, the particle displacement in the x direction is proportional to a_p^3.

Lastly, we consider the far-field. In the limit that $\xi \gg 1$ the transverse displacement close to the boundary tends to

$$\lim_{\xi\gg 1}\lim_{\zeta\to 1}\boldsymbol{\Delta r}_T^{(4)} = -\frac{945\pi\kappa Q_\perp}{32V^2H^4}\frac{\xi}{|\xi|^9} + O(\xi^{-9})\hat{\boldsymbol{e}}_y - \frac{315\pi\kappa Q_\perp}{4V^2H^4}\frac{1}{|\xi|^9} + O(\xi^{-10})\hat{\boldsymbol{e}}_x. \quad (6.6)$$

Therefore, it is clear that for large ξ values the $\kappa Q_\perp$ term will dominate and the κQ_r term will scale as $\xi^{-9,-10}$ in the y, x-directions respectively. Hence, the far-field will tend to that of figure 8b. This is contrary to the case of the free-slip boundary where the Q_r term governed the far-field of the transverse displacement, as shown in figure 6a.

Far away from the boundary and swimming path, in the limit $\zeta \to \infty$, the transverse displacement tends to

$$\lim_{\zeta\gg 1}\boldsymbol{\Delta r}_T^{(4)} = +\frac{1575\pi\kappa Q_r}{16V^2H^4}\frac{1}{\zeta^6} + O(\zeta^{-7})\hat{\boldsymbol{e}}_y + \frac{315\pi\kappa Q_\perp}{32V^2H^4}\frac{1}{\zeta^6} + O(\zeta^{-7})\hat{\boldsymbol{e}}_x. \quad (6.7)$$

These power laws for large ζ values are not the same as the results for large ξ and small ζ values as seen in equation (6.6). For the free-slip boundary the scaling in both limits, given by equations (5.8)-(5.9), are the same, *i.e.* $\boldsymbol{\Delta r}_T^{(4)} \sim Q_r/\xi^5 + Q_\perp\xi^6$. Hence, the higher decay powers in equation (6.7) re-emphasizes the point that the no-slip boundary suppresses the displacement, close to the boundary as well as in the far-field. Note that the Q_r and $Q_\perp$ terms become of equal scaling strength for large ζ values, so the $Q_\perp$ dominance disappears and both terms must be considered when conducting analysis.

To summarise, in the limit of tracers located close to a boundary and close to the finite swimming path so that $r_T^{int} \ll L$, the transverse tracer displacement consists of two terms proportional to κQ_r and $\kappa Q_\perp$ respectively, as for the free-slip boundary. Therefore we find that near a boundary both rotating and non-rotating swimmers generate mixing of particles in the transverse directions.

REFERENCES

Andrews, G. E., Askey, R. & Roy, R. 1999 Special functions, volume 71 of encyclopedia of mathematics and its applications.

Arfken, G. B. & Weber, H. J. 2005 *Mathematical Methods For Physicists International Student Edition*. Academic press.

Blake, J. R. 1971 A note on the image system for a stokeslet in a no-slip boundary. In *Proc. Camb. Phil. Soc*, , vol. 70, pp. 303–310. Cambridge Univ Press.

Ishikawa, T., Simmonds, M. & Pedley, T. 2006 Hydrodynamic interaction of two swimming model micro-organisms. *Journal of Fluid Mechanics* **568**, 119–160.

Kim, S. & Karilla, S. 1991 *Microhydrodynamics: principles and selected applications*. Butterworth series of chemical engineering.

Lorentz, H. 1896 Zittingsverslag. *Akademie van Wetenschappen 5* **168**.

Mathijssen, A. J. T. M. 2016 Phd thesis. *Manuscript in Preparation* .

Pozrikidis, C. 1992 *Boundary integral and singularity methods for linearized viscous flow*. Cambridge University Press.

Pushkin, D. O., Shum, H. & Yeomans, J. M. 2013 Fluid transport by individual microswimmers. *Journal of Fluid Mechanics* **726**, 5–25.

Vidūnas, R. 2009 Specialization of Appell's functions to univariate hypergeometric functions. *Journal of Mathematical Analysis and Applications* **355** (1), 145–163.

Yeomans, J. M., Pushkin, D. O. & Shum, H. 2014 An introduction to the hydrodynamics of swimming microorganisms. *The European Physical Journal Special Topics* **223** (9).